Bull. Astr. Soc. India (2000) **28**, 593–646

Magnetic reconnection

G. S. Lakhina

Indian Institute of Geomagnetism, Colaba, Bombay 400005, India

Received 10 January 2000; accepted 6 September 2000

Abstract Magnetic reconnection is considered as a basic plasma process which efficiently converts magnetic energy to plasma kinetic energy accompanied by changes in the topology of the magnetic field configuration. It prohibits the excessive build-up of magnetic energy in the current sheets encountered in astrophysical and space plasmas. Some of the important theories concerning magnetic reconnection are described in a simple manner. The difference between magnetic reconnection and diffusion is emphasized. The aim of this review is to high light the physical ideas of magnetic reconnection with the help of mathematical tools. For the purpose of illustration, applications of magnetic reconnection to solar flares and magnetospheric substorms are discussed.

Keywords: steady state reconnection, driven reconnection, current sheets, spontaneous reconnection, magnetic energy conversion, solar flare energy release, substorms, X-ray jets.

1. Introduction

Magnetic reconnection is recognized as a fundamental plasma process which converts magnetic energy into kinetic and internal energy of the plasma, and also allows the transfer of magnetic flux and mass between separate magnetic flux regions. The concept of magnetic field line reconnection appeared in connection with particle acceleration in solar flare. Giovanelli (1947) suggested that the conversion of the magnetic field energy in the flaring region into plasma kinetic energy could easily explain the energy released during solar flares. Dungey (1961) applied this idea to the interaction between the interplanetary magnetic field (IMF) and the Earth's magnetic field, the so called *dayside reconnection.* The dayside reconnection is considered as an important process for the exchange of energy,

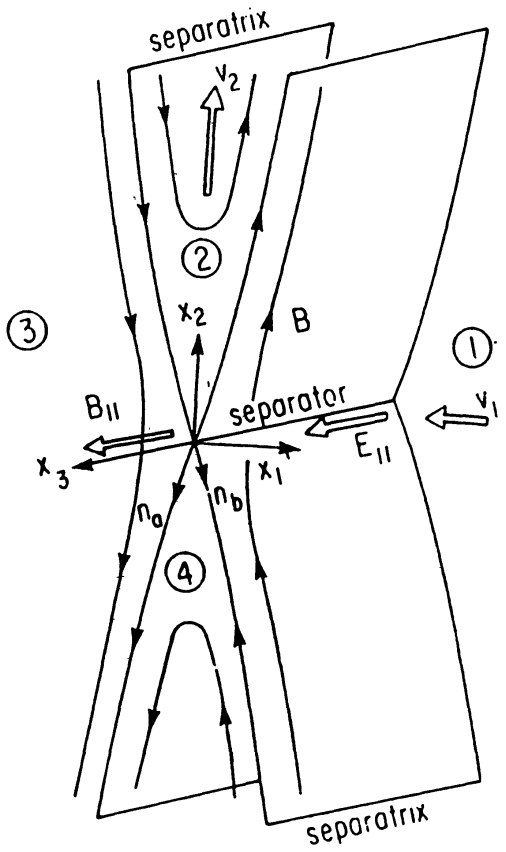

Figure 1. Basic magnetic field configuration for reconnection, 1 and 3 are the *inflow* regions, 2 and 4 are the *outflow* regions. Various *separatrices* divide space into regions of different magnetic field topology. A *separator* or X-line, which marks the intersection of two separatrix surfaces is also shown. Reconnection occurs when an electric field $\mathbf{E}$ exists along an X-line in a magnetic configuration.

momentum, and mass between the solar wind and the Earth's magnetosphere (Lakhina and Tsurutani, 1998a).

Magnetic field line reconnection is a process whereby plasma flows across a surface that separates regions containing topologically different magnetic field lines. This process changes the topology of the magnetic field. The magnitude of plasma flow is a measure of the reconnection rate Vasyliunas (1975). The essential feature of reconnection is the transfer of magnetic flux from the two *inflow regions* across the *separatrices* and into reconnected *outflow regions* as shown in Figure 1. Here regions 1 and 3 are the *inflow regions*, regions 2 and 4 are the *outflow regions*, and *separatrices* are the regions, which divide the space into region of field lines of different type. This process requires the existence of an electric field along a magnetic separator. A *separator* (or X-line) is a special type of field line that marks the intersection of separatrix surfaces. Therefore, according to Dungey (1978), reconnection occurs when an electric field $\mathbf{E}$ exists along an X-line in a magnetic field. The reconnection rate is proportional to E.

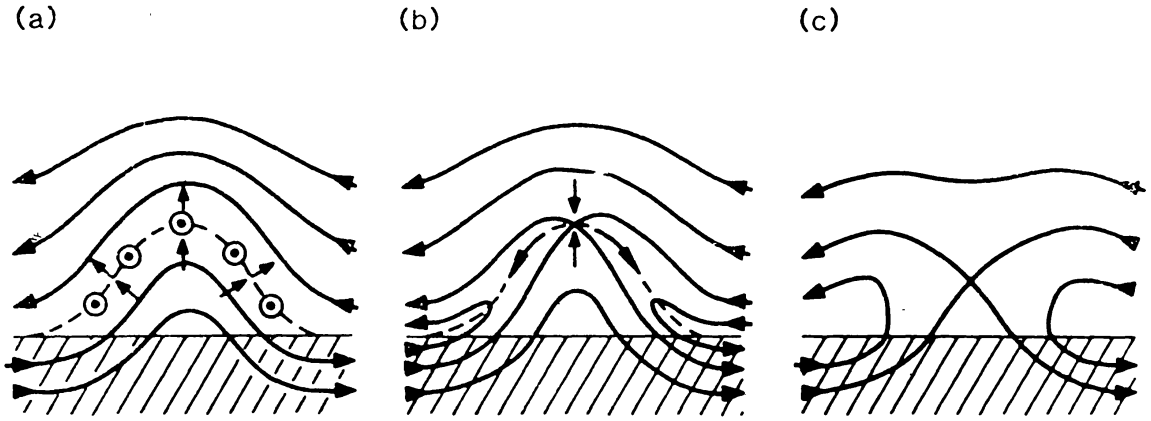

Figure 2. Schematic model for the magnetic reconnection on the Sun. Magnetic flux emerges from the solar photosphere (hatched region) and interacts with overlying coronal magnetic field and plasma. (a) In the frozen-field limit the two plasmas remain distinct and a thin current sheet (dashed line) forms between them. (b) Reconnection results in field interconnection and plasma mixing across the boundary current sheet. (c) The final stage is a potential field obeying the new photospheric boundary condition, which allows lower magnetic energy state, i.e., the magnetic energy is reduced compared to (a) having been fed into the surrounding plasma.

It is believed that magnetic reconnection can occur on the Sun heating the solar corona and producing solar flares (as shown schematically in Figure 2), in the Earth's magnetosphere producing flux transfer events and magnetospheric substorms (as shown in Figure 3), in comets giving rise to the phenomena of comet tail disconnections, in stellar accretion disks and galactic jets accelerating particles to high energies, and also in laboratory plasma devices like Tokamaks and Theta-pinches.

Magnetic reconnection involves the break down of magnetohydrodynamic *frozen field* concept. Dissipative terms, for example resistivity, which are normally negligible in large systems become locally dominant and produce dramatic changes in the large-scale flows and in the magnetic topology. Analytical theories of magnetic reconnection are based on essentially two approaches. In the first

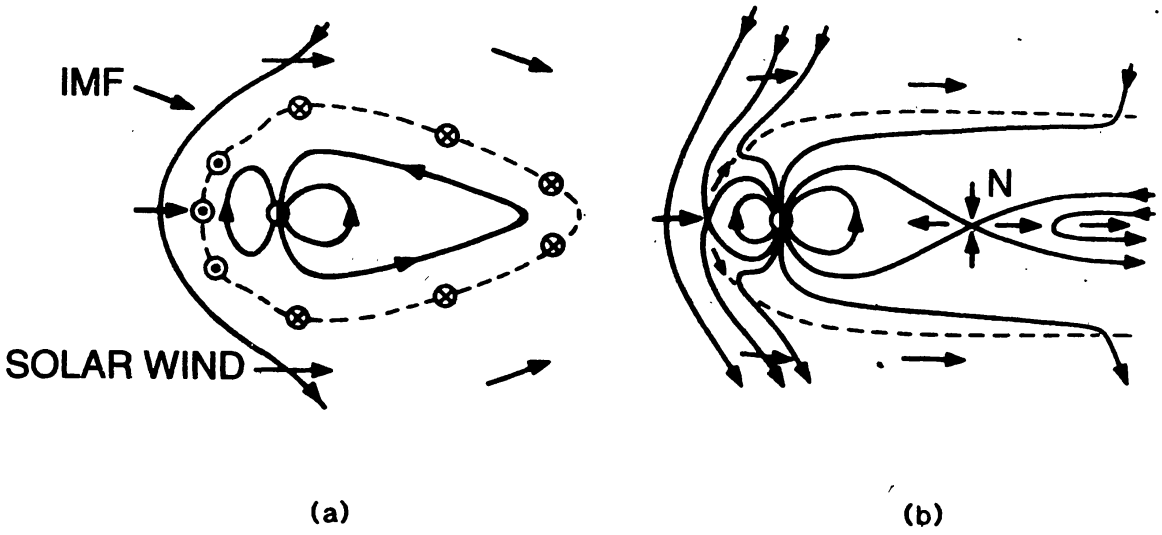

Figure 3. Schematics of the magnetic reconnection at the Earth's magnetosphere. (a) Magnetospheric model based on strict application of frozen-field theorem. (b) Magnetospheric model which allows reconnection between the interplanetary magnetic field and the geomagnetic field at the dayside magnetopause current sheet. The magnetic flux is eroded from the dayside and transported to the nightside by the solar wind. Stored magnetic energy in the magnetotail is explosively released during substorms, believed to be triggered by the onset of reconnection at the near Earth neutral line.

approach the process of magnetic reconnection is assumed to occur continuously in a steady state manner, this is called *steadily driven* or *forced reconnection.* Various aspects of steady state reconnection models have been developed by Sweet (1958), Parker (1957), Petschek (1964), Sonnerup (1970), and Yeh and Axford (1970). An excellent account of steady state reconnection models is given by Vasyliunas (1975), Axford (1984), Cowley (1985), and Forbes and Priest (1987). In the second approach the reconnection is treated as a time-dependent process, this is usually referred to as *spontaneous reconnection* or tearing mode instability. For time-dependent spontaneous reconnection, one can refer to an excellent review by Schindler (1984).

Before we proceed to discuss various theories of magnetic reconnection, we shall point out essential difference between ordinary diffusion and reconnection. It will be shown that diffusion dissipate the energy at a slow rate whereas the

reconnection proceeds at much faster rate converting the magnetic energy into plasma flow and thermal energy.

2. Diffusion versus reconnection

Let us consider a plasma obeying the simple Ohm's law of the form

$$\mathbf{J} = \sigma(\mathbf{E} + \mathbf{v} \times \mathbf{B}), \tag{1}$$

where $\mathbf{J}$, $\mathbf{E}$, $\mathbf{B}$, $\mathbf{v}$, and σ are respectively the electric current density, the electric field, the magnetic field, the plasma fluid velocity, and the electrical conductivity. The Faraday and the Ampere laws are,

$$\frac{\partial \mathbf{B}}{\partial t} = -\nabla \times \mathbf{E}, \tag{2}$$

$$\mu_0 \mathbf{J} = \nabla \times \mathbf{B}, \tag{3}$$

where μ_0 is the permeability of the medium. Combining Eqs. (2) and (3) with Eq. (1), we can arrive at,

$$\frac{\partial \mathbf{B}}{\partial t} = \nabla \times (\mathbf{v} \times \mathbf{B}) + \eta \nabla^2 \mathbf{B}, \tag{4}$$

where $\eta = (\mu_0 \sigma)^{-1}$ is the magnetic diffusivity. The behavior of the magnetic field depends on the relative importance of the two terms on the right hand side of Eq. (4). The first term describes *convection* of the field with the plasma flow. If the second term on the right hand side of Eq. (4) is negligible, then the magnetic field and the flow are *frozen* together such that a set of fluid elements which are initially located along a given field line remain so connected in all subsequent motion. This assumption is called the perfect conductivity approximation irrespective of the actual value of σ. The ideal magnetohydrodynamics description for a plasma is valid under this assumption.

When the second term on the right hand side of Eq. (4) is dominant, this equation becomes a *diffusion* equation. It, then, describes the diffusion of the magnetic field lines through the plasma down the field gradients, such as to reduce those gradients (i.e., the current densities). There is then essentially no coupling between the field and the fluid flows.

The relative magnitude of the convective term and the diffusion term on the right hand side of Eq. (4) is the *magnetic Reynolds number*, R_m, which can be written as

$$R_m = \frac{|\nabla \times (\mathbf{v} \times \mathbf{B})|}{|\eta \nabla^2 \mathbf{B}|} = \frac{VL}{\eta}, \tag{5}$$

where V and L are respectively the characteristic speed in the flow and the length scale of the magnetic field configuration. If $R_m \gg 1$, convection dominates and

the *frozen-in flow* prevails, while if $R_m \ll 1$, diffusion dominates and the coupling to the plasma is weak. In astrophysical plasmas R_m is very large as the overall spatial scales of the plasma systems are very large. For example, we get $R_m = 10^8$ for the solar flares, and $R_m = 10^{10} - 10^{11}$ for the solar wind and the magnetosphere when we take L as the overall size of the plasma system. This shows that on large spatial scales (e.g., $L \sim 10^4$ km for solar flares, a few solar radii for the solar wind, and a fraction of the cavity radius for the planetary magnetospheres) magnetic field convection is overwhelmingly dominant and the effect of diffusion can be entirely neglected. Observations of magnetically ordered plasma structures in the coronal loops, the spiral structure of the interplanetary magnetic field, and the magnetic organization of the planetary magnetospheres provide evidence for the validity of this statement.

However this is not the complete story. The above conclusions that diffusive processes can be neglected in astrophysical plasmas are based on the consideration of the overall size of the plasma system as the characteristic length scale L. Since the characteristic length that must be considered pertains to the magnetic field rather than the entire configuration, it is possible for a situation to arise in which L is locally small, e.g., in a local region of magnetic field reversal, or a current sheet. In this case, the time-scale for diffusion of magnetic field lines relative to the fluid is $t_d = L^2/\eta$. When t_d becomes comparable with the time-scale for the removal of the field lines from the locality $t_A = L/V_A$, where $V_A = B(\mu_0\rho)^{-1/2}$ is the Alfvén speed, then the *frozen field* concept becomes locally invalid. In such circumstances, the magnetic field lines can be described as *reconnecting* in this localized *diffusion* region where $t_d/t_A = LV/\eta = R_m = 1$. Note that outside the diffusion region, R_m could be very large, and the *frozen field* concept would generally hold. However, if fluid elements which are at one time connected by a common magnetic field line pass through a *diffusion* region (where *frozen field* theorem breaks down completely), they will become disconnected from each other, and connected afterwards to different sets of fluid elements. This process of *partner swapping* or *reconnection* is shown in Figure 4.

2.1. One Dimensional Current Sheet

Let us consider a one - dimensional current sheet with $\mathbf{B}$= B(x,t) $\hat{y}$, as shown in Figure 5, in hydrostatic equilibrium i.e., with the flow velocity $\mathbf{v} = 0$. The initial ($t = 0$) magnetic field configuration contains a discontinuity which is a current sheet at $x = 0$ with $B(x, 0) = \pm B_0$, where the plus (+) sign before B_0 corresponds to the region $x > 0$ and the minus (-) sign to the region $x < 0$. In such a case, Eq. (4) reduces to

$$\frac{\partial B}{\partial t} = \eta \frac{\partial^2 B}{\partial x^2} \tag{6}$$

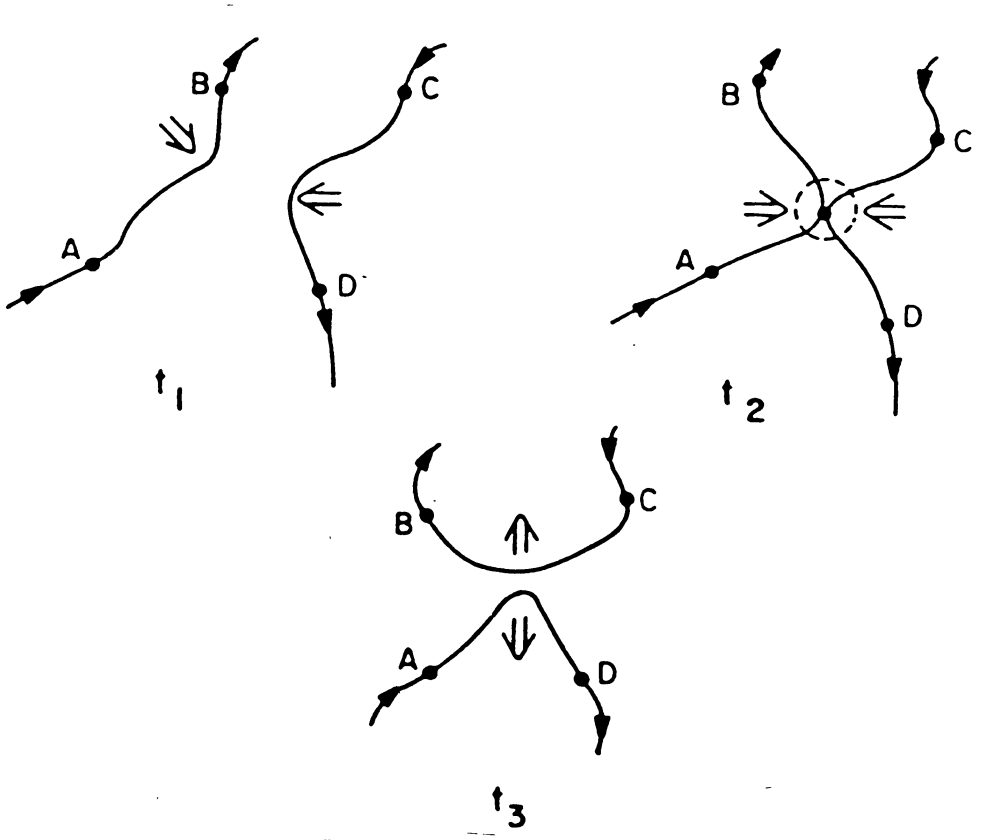

Figure 4. A simple illustration of the reconnection process in a conducting fluid. At time t_1 the magnetic field line defined by fluid elements A and B approaches a more or less oppositely-directed field line defined by fluid elements C and D. At time t_2 the two field lines touch at some point. At time t_3 the connection between A and B and between C and D is broken due to reconnection process occurring in the localized region where the two lines touch each other. Consequently, the field line defined by the fluid elements A and D moves away from the field line defined by the fluid elements B and C

Equation (6) is a pure diffusion equation whose solution may be written as

$$B(x,t) = \int G(x'-x,t)B(x',0)dx', \tag{7}$$

where G is the Green's function,

$$G(x'-x,t) = (4\pi\eta t)^{-1/2}\exp[-(x'-x)^2/4\eta t] \tag{8}$$

For the case of an infinitely thin current sheet with a piecewise constant B as defined above, we get the solution

$$B(x,t) = \frac{2B_0}{\sqrt{\pi}}\mathrm{erf}\left[\frac{x}{(4\eta t)^{1/2}}\right], \tag{9}$$

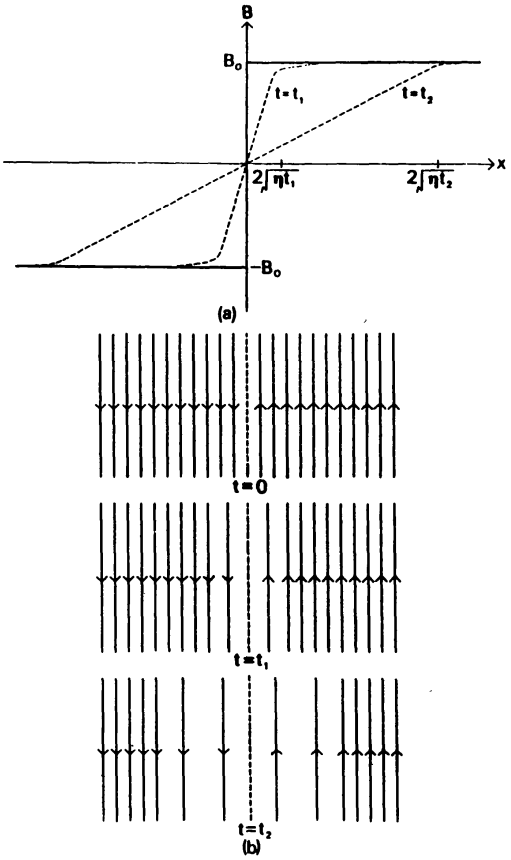

Figure 5. A diffusive current sheet: (a) variation of the magnetic field strength with space, (b) a sketch of the magnetic field lines at three different times.

where the *error function* is defined as

$$\mathrm{erf}(\xi) = \int_0^{\xi} e^{-z^2}\, dz. \tag{10}$$

¿From solution (9), we note that half thickness of diffusion region l is simply given by $l = (\eta t)^{1/2}$ which increases with time as $t^{1/2}$ as shown in Figure 5. The resulting magnetic field at fixed position decreases with time and the field is said to be *annihilated.* This means that magnetic energy is simply converted into heat by Ohmic dissipation (cf. Figure 6a). Furthermore, we note that pure diffusion is a self-limiting process as a means of rapidly converting magnetic energy into heat and kinetic energy since it simultaneously reduces strong field gradients. The rate of diffusion η/l falls sharply as l increases with time.

This situation can dramatically change when the flows are present (cf. Figure 6b). In such a case the magnetic field diffusion rate could be kept at a high level provided the fluid moves towards the diffusion region (current sheet) to maintain the field gradients. Thus, faster the inflow, steeper are the gradients required (i.e., the current sheet becomes thinner), and larger is the rate of energy liberated

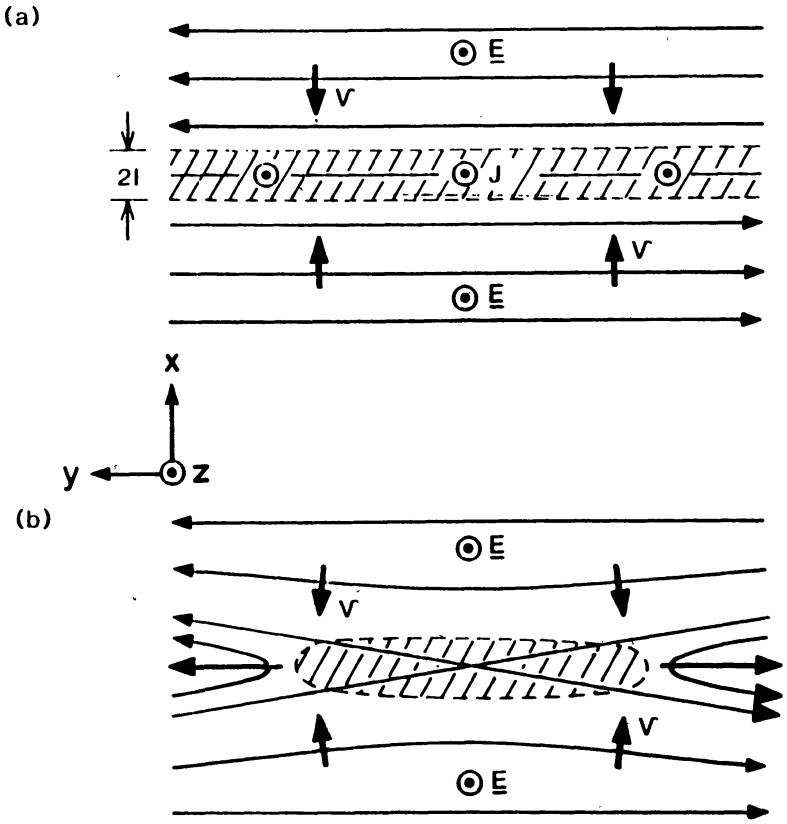

Figure 6. Schematics of the magnetic field (solid lines) and flow geometry (arrows) appropriate to (a) field annihilation and (b) magnetic reconnection. The diffusion regions where finite conductivity is important is shown by the hatched areas, surrounded by the unhatched convection regions. The directions of the electric field and current flow out of the diagram are shown by the circled dots.

from the magnetic field to the plasma. The half-width l of the equilibrium current sheet for a given inflow speed V_i may be calculated by equating the rate at which the flux is convected into the current sheet from each side, to the rate of flux annihilation in the diffusion region. This gives

$$V_i B_0/l = \eta B_0/l^2 \quad \text{or} \quad l = \frac{\eta}{V_i}. \tag{11}$$

The magnetic Reynolds number for the current sheet based on l defined by Eq. (11) comes out to be

$$R_m = \frac{V_i l}{\eta} = 1. \tag{12}$$

This means that the sheet width is just sufficiently small that diffusion and convection are equal in importance, as should be expected from the steady state situation. Under the condition that V is constant through out on either side of

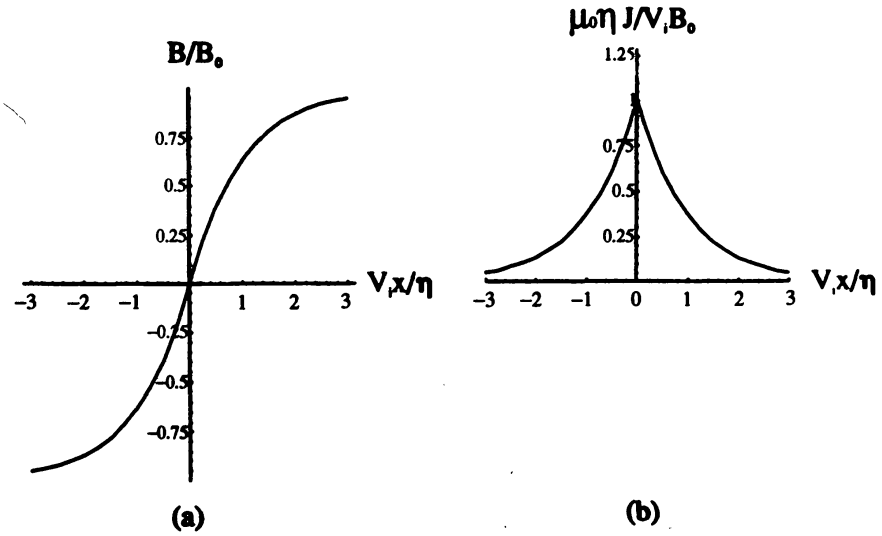

Figure 7. Plot of the variation of (a) the magnetic field B/B_0 , and (b) the current density $\mu\eta J_z/V_iB_0$ versus xV_i/η from the solution as given by Eq. (13).

the current sheet, i.e., $\mathbf{v} = \mp V_i\hat{x}$, and assuming $B(x = \pm\infty) = \pm B_0$, we can write down the steady state solution of Eq. (4), satisfying condition (12), as

$$B = \pm B_0[1 - \exp(\mp V_i x/\eta)], \tag{13}$$

where the upper and lower signs refer to $x > 0$ or $x < 0$ respectively. The solutions for B and the corresponding current density calculated by using the Ampere's law are shown in Figure 7. The current density is concentrated in a thin layer around $x = 0$, and falls off exponentialy with increasing x.

We may point out that solution given by Eq. (13) is not realistic as the assumption of constant V is rather unphysical. Sonnerup and Priest (1975) have obtained a realistic solution of the steady state annihilation problem in a one-dimensional current sheet with a stagnation-point (hyperbolic streamlines) flow as shown in Figure 8. Physically what happens is the following: suppose that magnetic flux is carried by the plasma motion towards the plane $x = 0$ from both sides at a constant speed V_i. Then according to Eq. (11), a steady state current sheet of half-width $l = \eta/V_i$ can exist in which the outwards diffusion of

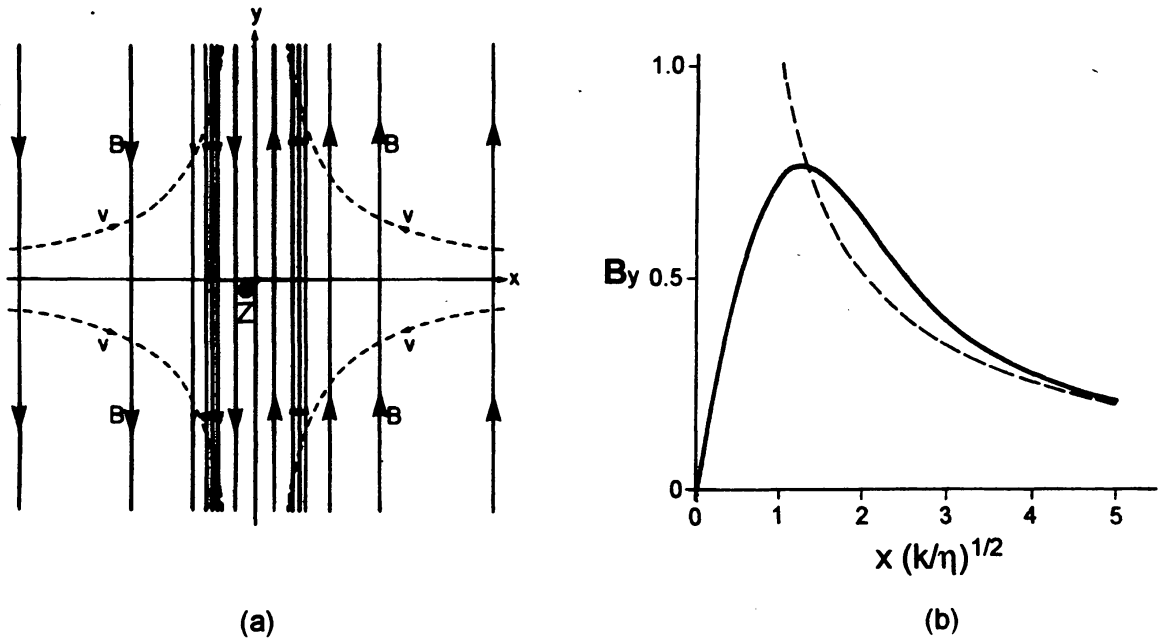

Figure 8. (a) Oppositely directed field lines (solid lines) are carried in from the two sides by a stagnation point flow with streamlines shown as dashed lines. When the field lines enter the current sheet or diffusion region, centered at $x = 0$, they are no longer frozen to the plasma. In the diffusion region they are annihilated, while the magnetic energy is converted to heat by Joule dissipation. The configuration is a steady one provided the diffusion region width is such that outwards diffusion of field lines is balanced by their inwards convection. (b) The resulting magnetic field strength as a function of x expressed in units such that the gradient dB_y/dx is unity at the origin. The dashed line represents the solution, $B_y = E(kx)^{-1}$, where $k = V/l$ and l is the half-width of the currentsheet, when diffusion is neglected.

the magnetic field is balanced by the inward convection of new flux. However, plasma will be carried in with the flux, and this must be turned away and flow out along the sheet to prevent pile-up of matter near the neutral line, as shown in Figure 8.

We must emphasize that the one-dimensional annihilation systems discussed here suffer from two main drawbacks. Firstly, we have plasma inflow into the current sheet from either side, but we have ignored the question of its exit from the current sheet. Secondly, no proper treatment for the structure of the magnetic field and flow in the diffusion region is done. These important question are dealt with in various steady state reconnection models.

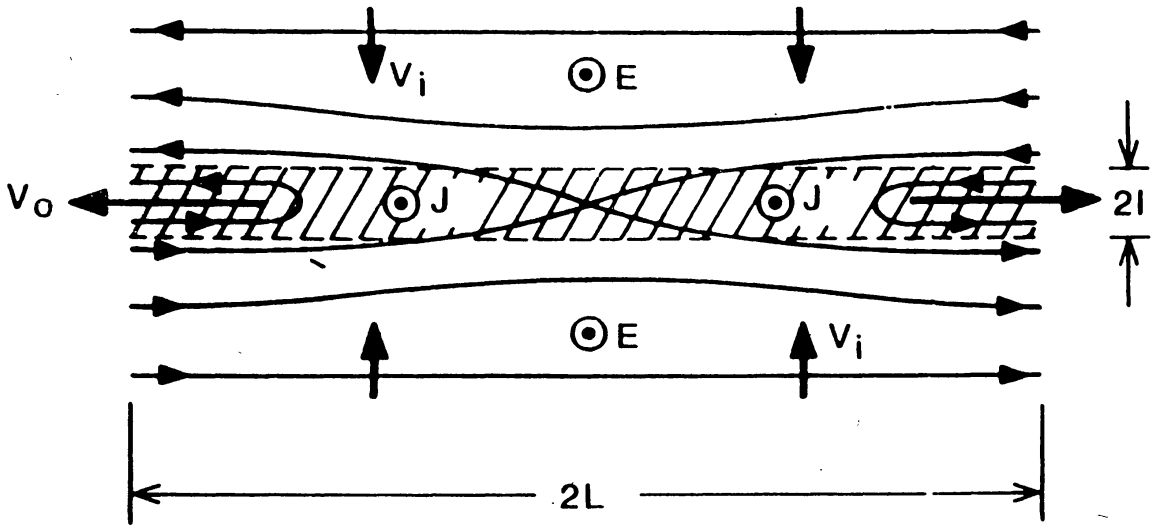

Figure 9. Sketch of the field lines (solid lines) and flow configuration (arrows) assumed in the Sweet-Parker model. The current sheet (or diffusion region) shown hatched, has the small half-width l set by the scale of diffusion over its whole half-width L which is taken as the scale size of the system.

3. Steady State Reconnection Models

Most of the steady state reconnection models are based on the magnetohydrodynamic (MHD) theory. The basic philosophy of all the MHD models is to break the flow into two parts: an inflow (or outer) region in which the electrical conductivity is considered infinite so that *frozen field* theorem applies, and an out flow (i.e., inner) region – the diffusion region– surrounding the separator in which resistive and other dissipative effects are taken into account. The solutions in these two regions are, then, matched appropriately depending on the boundary conditions. We shall discuss first the *classical* solutions of *Sweet and Parker* (Parker, 1957; Sweet 1958) which formed the basis of later models.

3.1. Sweet-Parker Model

The main features of the field and flow configurations for this model are shown in Figure 9. The configuration is two-dimensional. The steady state reconnection is

maintained by the balance between the plasma inflowing into the diffusion region of width $2l$ and the equal outflowing plasma along the current sheet of length $2L$. For simplicity, we consider the magnetic fields to be antiparallel, and the plasma to be incompressible. The plasma flows towards the current sheet from both sides with inflow speed, V_i, and flows out along the current sheet at speed V_o.

The balance between convection of flux into the current sheet and flux annihilation due to diffusion within it determines the width of the diffusion region, and it is given by Eq. (11). It is assumed that diffusion region extends all along the length $2L$ of the current sheet. If the density is assumed constant, then the conservation of the mass requires

$$\nabla \cdot \mathbf{V} = 0 \quad \text{or} \quad V_i L = V_o l. \tag{14}$$

The total pressure $(p + B^2/2\mu_0)$ is constant across the sheet, as seen from the momentum equation. It means that

$$p_o = p_i + \frac{B_i^2}{2\mu_0}, \tag{15}$$

where p_o is plasma pressure on the central plane where B goes through zero. The pressure difference $(p_o - p_i)$ ejects the fluid from between the two opposing fields along the current sheet as shown in Figure 9, with a velocity given by,

$$V_o = \left[\frac{2(p_o - p_i)}{\rho}\right]^{1/2} = \frac{B_i}{(\rho\mu_0)^{1/2}} \equiv V_{Ai} \tag{16}$$

where V_{Ai} is the Alfvén velocity. Then, from Eqs. (11), (14) and (16), we get an expression for the reconnection rate as,

$$V_i = \frac{V_{Ai}}{R_M^{1/2}}, \tag{17}$$

where $R_M = (V_{Ai}L/\eta)$ is the magnetic Reynolds (or Lundquist) number based on the inflow Alfvén speed (which in this case happens to be the plasma out flow speed), and overall system scale length L. Note that if the fields were in the same direction, instead of opposite direction, then the smallest scale would be L instead of l. In that case the characteristic diffusion velocity would be $V_d = \eta/L = V_{Ai}/R_M$ (cf. section 2.2). Thus the rate V_i given by Eq. (17) at which the opposite fields reconnect is larger than the passive diffusion rate V_d by a factor of $R_M^{1/2}$. Since R_M is very large compared to 1 in astrophysical plasmas (e.g., $R_M = 10^8$ in solar flares etc.), the resistive dissipation and reconnection is enhanced by a large factor. Even then, as seen from Eq. (17), the rate of reconnection, i.e., the inflow speed V_i, is still very small compared to the Alfvén speed , V_{Ai}, by the same large factor $R_M^{1/2}$. In other words, according to Sweet-Parker models, the liberation of the magnetic energy to the plasma occurs very slowly.

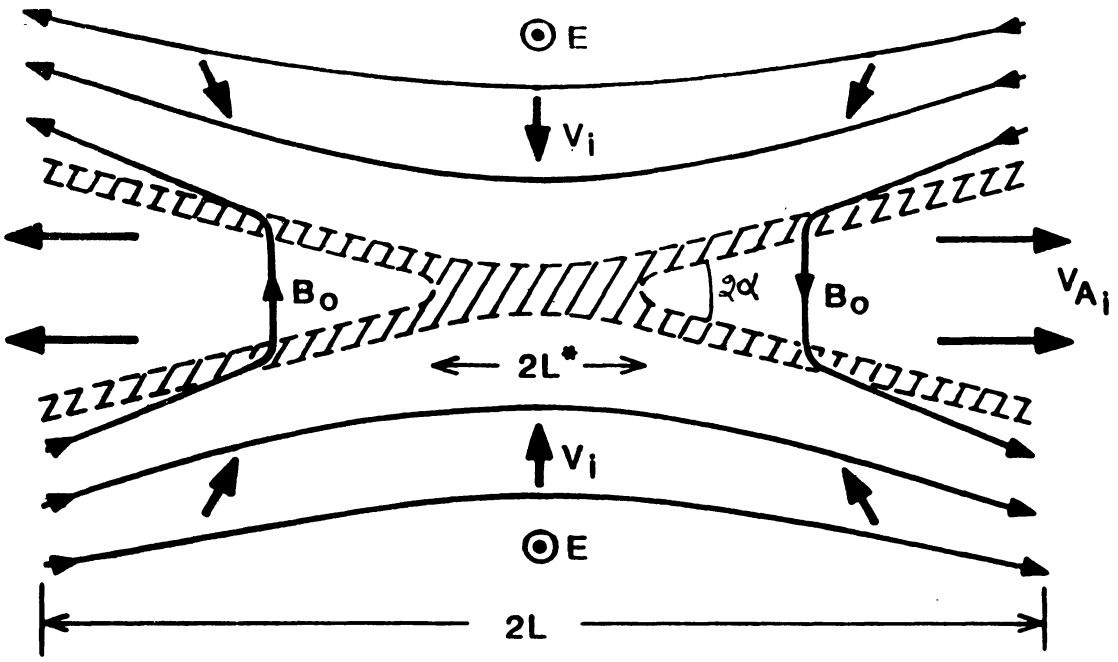

Figure 10. Schematics of the magnetic field and plasma flow configuration (solid lines and the arrows respectively) in the Petschek model. A small central diffusion region of length $2L^*$ surrounding the neutral line bifurcates into two standing-wave current sheets in the downstream flow (current-carrying regions are shown as hatched). Most of the inflowing plasma is accelerated to a speed $\simeq V_{Ai}$ along the boundary between the two inflows as it crosses these standing-waves.

3.2. Petschek Model

The reason for small reconnection rate in *Sweet-Parker* mechanism is due to the fact that the length of the diffusion region is equal to the system length L which is very large compared to its width l. This can be easily verified from Eq. (14) which demands $V_i = (l/L)V_{Ai} \ll V_{Ai}$, and hence the low rate of reconnection.

Petschek (1964) suggested that if the opposite fields meet only over a narrow length L^*, rather than all along the system length L (as shown in Figure 10), then the reconnection rate could be considerably enhanced. The conservation of fluid over the diffusion region, then, would demand

$$V_i = \frac{l}{L^*} V_{Ai} \tag{18}$$

In particular, if $L^* \simeq l$, one can have $V_i \simeq V_{Ai}$, which would be a rapid reconnection indeed! The question is whether nature would have it so?

Petschek (1964) pointed out that the ideal MHD flow in the outer region is expected to contain standing MHD waves fronts as shown in Figure 10, where these fronts are *slow-shocks*. Two standing Alfvén shocks deflect and accelerate the incoming plasma into two exit jets wedged between the shocks. A diffusion region still surrounds the neutral line, however, constituting a miniature (in length) *Sweet- Parker* system. The magnetic energy could be converted to plasma energy as a result of slow Alfvén shocks as well as due to diffusion.

Let us denote by α the half-angle of the exit flow (cf. Figure 10). This angle α can be determined by the requirement that the slow Alfvén waves remain stationary in the flow. In the incompressible case the required condition is that the plasma flow speed normal to the plane of the wave should be equal to the Alfvén speed based on the magnetic field component also normal to the plane of the wave. The laws of conservation of the flux (i.e., $V_i B_i = V_o B_o$), and tangential stress (i.e., $\rho V_i V_o = B_i B_o/\mu_0$) demand that the outflow speed be $V_o = V_{Ai}$ parallel to x-axis as in Sweet - Parker model. Then, the normal flow speed would be $V_n = V_{Ai} \sin\alpha$, and the normal magnetic field component would be $B_n = B_o \cos\alpha$. Therefore, the requirement for the stationarity of the slow shocks in the flow would be met when

$$\tan\alpha = \frac{B_o}{V_{Ai}\sqrt{\mu_0 \rho}} = \frac{V_i}{V_{Ai}}, \tag{19}$$

where we have made use of the law of conservation of the magnetic flux. For $V_i \ll V_{Ai}$, the half-angle α of the narrow wedge is quite small, but when the inflow speed V_i increases, the angle also increases to accommodate the increased flow. For $V_i \sim V_{Ai}$, the half-angle would be $\alpha \simeq \pi/4$. The reason for this greatly increased reconnection rate in this case in contrast to *Sweet - Parker* case is that the flow is not constrained to flow out from a narrow channel of constant width l; rather the outflow occurs in an expanding wedge whose angle would change according to the inflow rate.

However, in reality there exists an upper limit to the reconnection rate in Petschek's system. Note that Eq. (19) has been derived by assuming that both B_i and V_i are constant throughout the inflow region starting from $x = \pm\infty$ and extending upto the boundary of the diffusion region. Since the electric field is uniform in the steady, two-dimensional configuration shown in Figure 10, it immediately follows that

$$V_i B_i = V_\infty B_\infty, \tag{20}$$

where V_i and B_i are identified as the flow and magnetic field strength at the diffusion region, and V_∞ and B_∞ are the flow speed and the magnetic field at $x = \pm\infty$. For $V_i \ll V_{Ai}$, angle α is small (cf. Eq. (19)), and the flow in the entire inflow region remains uniform with $V_i = V_\infty$. Now, as the flow speed V_i increases, so the inclination angle α of the shock wave increases, which in turn decreases the field strength at the diffusion region, i.e., $B_i < B_\infty$, by rotating the magnetic field vector towards the normal. This would speed up the inflow

resulting in $V_i > V_\infty$ as seen from Eq. (20). Hence, if the inflow speed increases beyond a maximum value, the field strength B_i is reduced to zero and the flow chokes off completely.

Petschek (1964) assumed that the plasma currents in the inflow and outflow regions outside the standing waves can be neglected as the flow is only weakly perturbed in these regions. Then, the magnetic field can be considered as a potential field. If the field strength is uniform ($B_\infty \hat{y}$) at large distances along x, and has a uniform vertical component $B_o \hat{x}$ along the length L in y- direction, then the magnetic field strength just outside the diffusion region, following Vasyliunas (1975), can be written as:

$$B_i = B_\infty - \frac{4B_o}{\pi} \ln\left(\frac{L}{r}\right), \tag{21}$$

where $r = (x^2 + y^2)^{1/2}$. The assumption that the inflow in the external region is weakly perturbed requires that the magnetic field perturbation not be large even in the vicinity of the reconnection region. Choosing $B_i(x = l, y = 0) = B_\infty/2$ in Eq. (21), gives

$$B_0 = \frac{\pi}{8} \frac{B_\infty}{\ln(L/l)}. \tag{22}$$

From Eq. (17) and (18), we get $L/l = R_M^{1/2}$. Then the upper limit on the reconnection rate, V_i^*, is obtained by assuming that $V_i^* B_\infty \approx V_o B_o = V_{Ai} B_o$, this gives

$$V_i^* = \frac{\pi}{8} \frac{V_{A\infty}}{\ln(R_M^{1/2})} = \frac{\pi}{4} \frac{V_{A\infty}}{\ln(R_M)}, \tag{23}$$

where R_M is defined with respect to the speed $V_{A\infty}$. Thus, for the appropriate boundary conditions, it is possible to reach a fairly high reconnection rate, i.e., $V_i = (0.01 - 0.1)\ V_{A\infty}$ in astrophysical plasmas by the Petschek model. An exact solution of the Petschek model for $M_A = V_i/V_{A\infty}$ is shown in Figure 11.

3.3. Sonnerup Model

In the Petschek (1964) model, the flow in the inflow region is convergent, i.e., $B_i < B_\infty$ and $V_i > V_\infty$. This is a characteristics of the fast mode waves in the inflow region. On the contrary, the inflowing plasma can support the slow mode wave which would produce diverging flows near the reconnection site as shown in Figure 12 (see also Figure 8). In Petschek model, the slow waves are excluded as the perturbed currents are neglected in the inflow region.

Sonnerup (1970) found a simple solution for the incompressible reconnection problem that consists entirely of a set of standing slow-mode waves separating wedges of uniform flow and field. The solution is shown in Figure 13. In this figure the standing waves are shown as small-dashed lines and the small diffusion

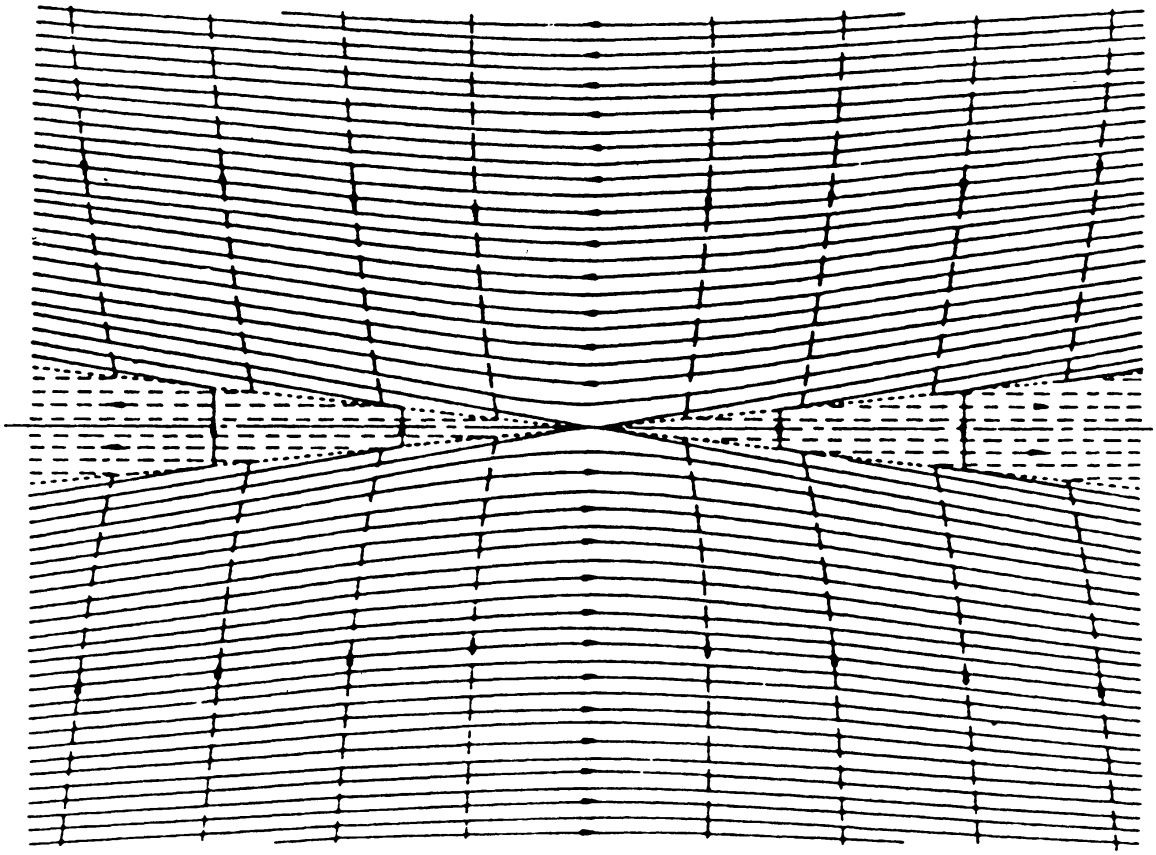

Figure 11. The *Petschek* [1964] solution drawn to a scale for the case $V_i/V_{Ai} = 0.1$ (from *Vasyliunas* [1975]). The magnetic field lines are solid and the plasma flow streamlines are dashed. Slow shocks, which intersect at the reconnecting regions, are shown by dotted lines. Note that the flow converges towards the reconnecting region so that $B_i < B_\infty$ and $V_{Ai} < V_{A\infty}$.

region is not shown. The basic property of this model is the appearance of slow-mode rather than the fast-mode expansion in the inflow region. The condition for the existence of these standing slow-mode waves is the same as that stated earlier for the Petschek model, i.e., $V_n = \pm B_n/\sqrt{\mu_0 \rho}$, where the subscript n denotes the component normal to the plane of the wave. The angles of inclination of these waves are determined by the requirement (in the symmetrical case) that both the magnetic field and the flow velocity (flow streamlines are shown as dashed lines with arrow in Figure 13) are rotated through a right angle between the inflow and the outflow regions. In order to accomplish this, at least two standing Alfvén waves are needed in each quadrant of the solution as shown in Figure 13 (small-dashed lines). The four waves near the boundary, bounding the central outflow region, correspond to Petschek's waves since consideration of the angle, α_P, at which these waves lie relative to the flow shows that they originate in the central diffusion region and propagate outwards along the reconnected field lines. Similar considerations applied to the four outer waves, i.e., Sonnerup's

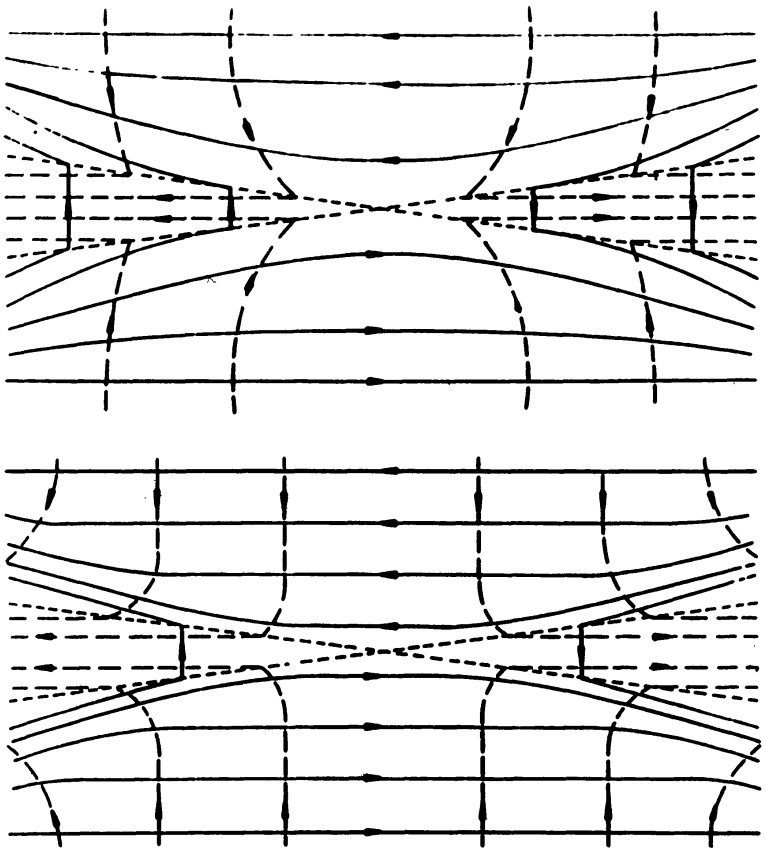

Figure 12. A schematic diagram showing the magnetic field lines (solid lines), plasma flow streamlines (dashed lines), and slow mode shocks (dotted lines) for the cases when the external flow corresponds to (top) a fast mode expansion, and (bottom) a slow mode expansion.

waves with inclination angle α_S, however, show that they must be generated in the outer part of the flow at the *corners* shown in Figure 13, and then propagate in towards the diffusion region.

Exact analytical solutions for the field and flow in each region together with the wave angles α_P and α_S can be readily found from the jump conditions across the standing wave discontinuities. In particular, if the plasma speed and the Alfvén speed in the inflow regions are V_i and V_{Ai} respectively, then from Eq. (19) we get

$$\tan \alpha_S = \frac{V_i}{V_{Ai}}, \tag{24}$$

for the Sonnerup waves. Calculations of α_P, V_o, and B_o are little more involved but straight forward, and following *Sonnerup* [1970], we can write the following relations:

$$\tan \alpha_P = \frac{V_i}{(\sqrt{2}+1)^2 V_{Ai}},$$

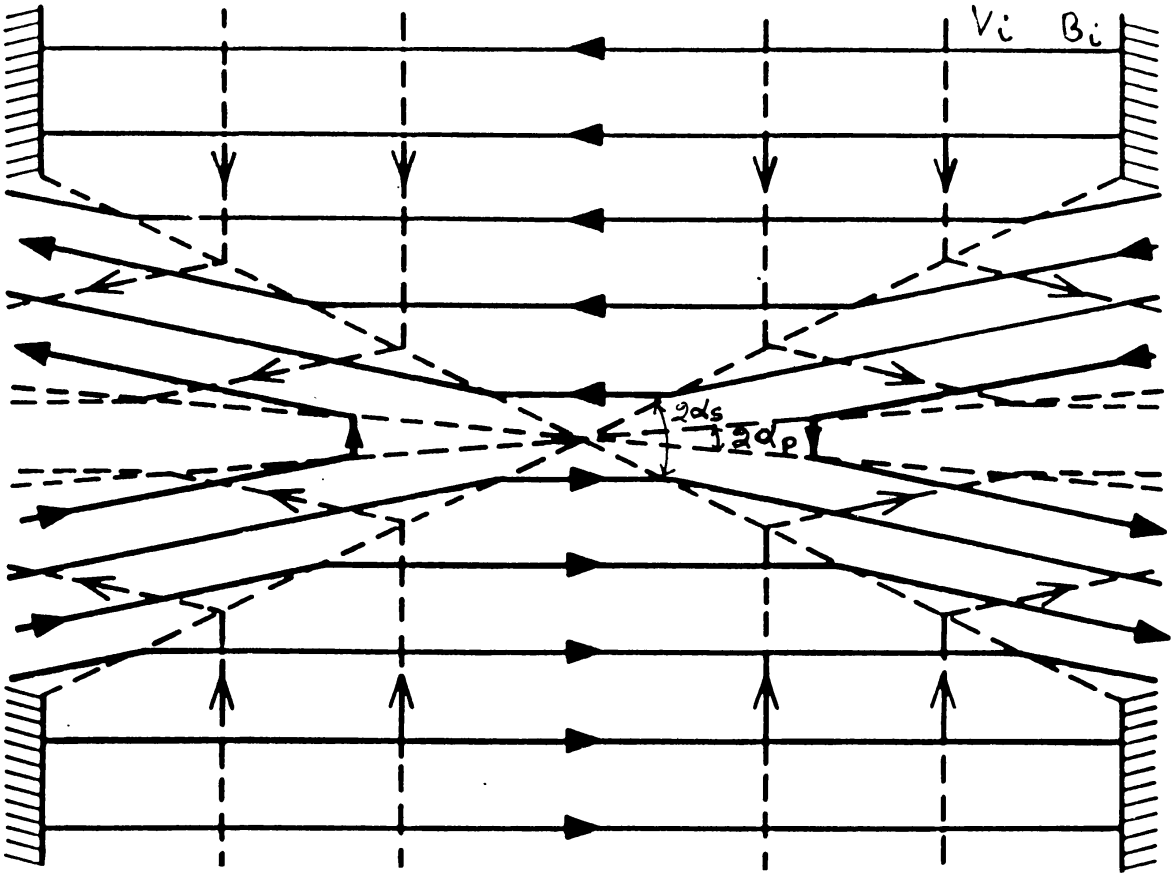

Figure 13. The Sonnerup convection region model for $V_i = 0.5\, V_{Ai}$. Magnetic field lines are shown by solid lines, flow streamlines by long-dashed lines with arrows, and the standing waves by short-dashed lines. The inflow may be considered to take place between plane parallel walls (shown hatched), while the outflow takes place through gaps in the walls. The outer waves originate at the gap edges, and the width of the gaps determines the inflow (and reconnection rate). The central diffusion region is not shown.

$$\begin{aligned} V_o &= (\sqrt{2}+1)V_{Ai}, \\ B_o &= (\sqrt{2}-1)\sqrt{\mu_0 \rho} V_i. \end{aligned} \tag{25}$$

From Eqs. (24)-(25), it is seen that for $V_i < (\sqrt{2}+1)V_{Ai}$, we have $B_o < B_i$ and $V_o > V_i$, which implies that magnetic energy is being converted to plasma kinetic energy. The maximum reconnection rate comes out to be $V_i = (\sqrt{2}+1)V_{Ai}$. However, at this maximum rate the inflow and the outflow region would become identical and there is no net energy exchange between the plasma and the field. An exact compressible solution to the above problem has been discussed by Hameiri (1979). In Hameiri's solution all slow-mode waves are replaced by rotational discontinuities. The conversion of energy from magnetic field to plasma can occur only in the diffusion region as the magnitude of the magnetic field is constant everywhere else.

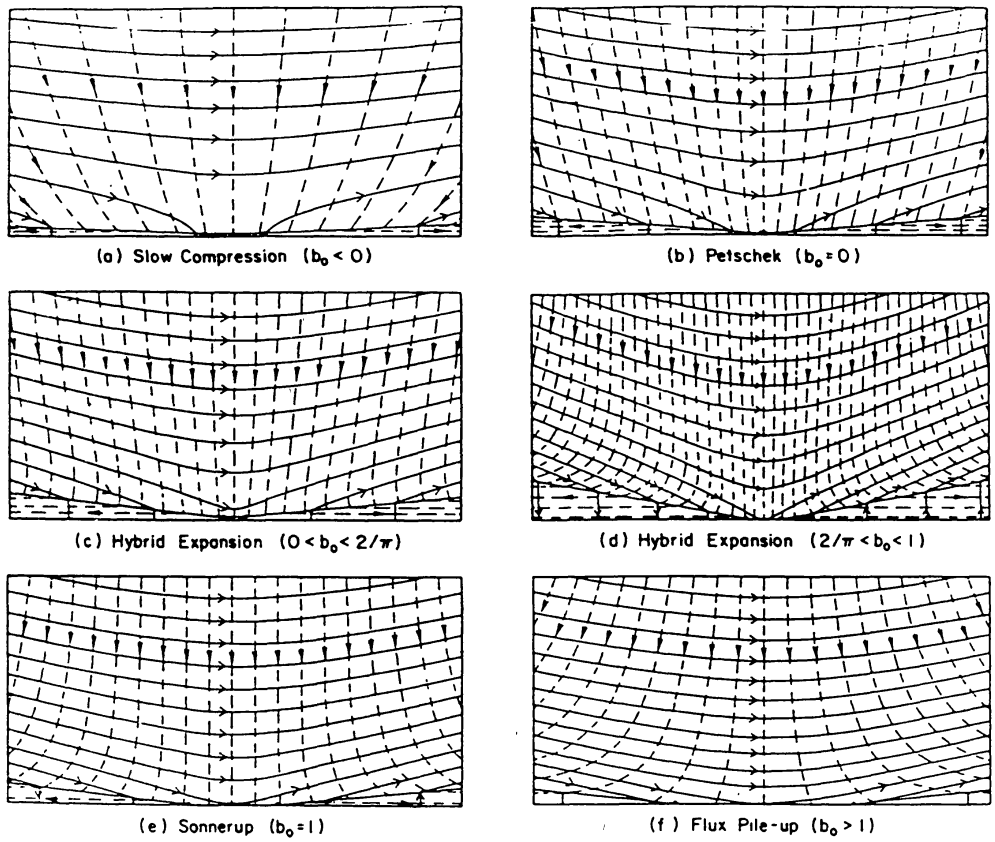

Figure 14. Unified family of linear models for incompressible, steady-state magnetic reconnection: (a) slow expansion model, (b) Petschek model, (c) hybrid expansion model for $0 < b_0 < 2/\pi$, (d) hybrid expansion model for $2/\pi < b_0 < 1$, (e) Sonnerup model, and (f) flux pile-up model [after *Priest and Forbes*, 1986].

Priest and Forbes (1986) have discussed a unified linear theory of steady state two-dimensional reconnection which brings out the inter-relation between the various reconnection models as shown in Figure 14. Their model is based on a similar expansion as in Petschek's model with a field diffusion region and outflow region. Their results depend on the parameter b_0, which characterizes the plasma flow at the inflow boundary. Petschek's model corresponds to $b_0 = 0$, and Sonnerup's model is recovered for $b_0 = 1$. On the other hand, some other reconnection models, such as a slow compression for $b_0 < 0$, a hybrid expansion model for $2/\pi < b_0 < 1$, and a flux pile-up model for $b_0 > 1$ are also obtained by their analysis. Yan et al. (1992) have obtained the various regimes predicted by Priest and Forbes (1986) in their simulations. They simulated cases which correspond to Petschek's fast-mode expansion model ($b_0 = 0$), Sonnerup's slow-mode expansion ($b_0 = 1$), Slow-mode compression ($b_0 = -4$), and flux pile-up model ($b_0 = 2$). Their simulation results for Petschek's model are shown in Figure 15. Two pairs of slow shocks are present in the region where the streamlines are

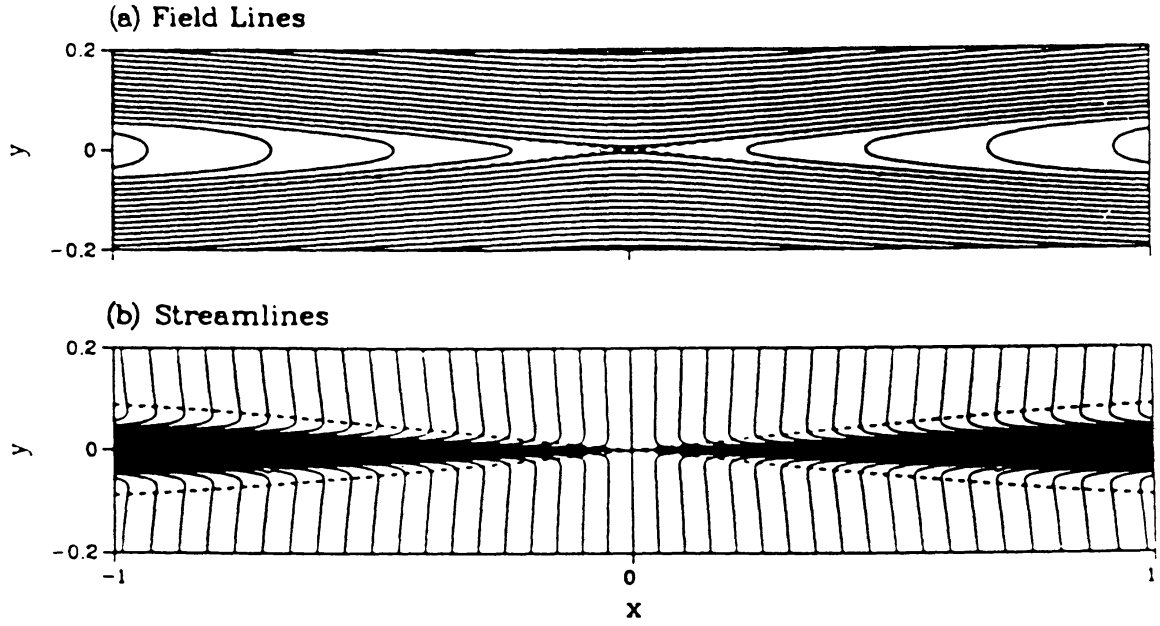

Figure 15. Magnetic field lines (upper panel) and streamlines of plasma flow (lower panel) as obtained in MHD simulation of Petschek's model. Dashed lines are the separatrices. Slow-shocks are located downstream of the separatrices [after *Yan et al.*, 1992]

highly bent (lower panel). The reduced magnetic fields and accelerated plasma flows in the region downstream of the slow shocks are indicative of magnetic energy being converted to plasma kinetic energy.

4. Spontaneous Reconnection

Spontaneous reconnection occurs when an originally stable system, gradually undergoing changes by external forces, passes over an onset point of an instability involving magnetic reconnection. The prototype of the instability is the *tearing mode* of a plane plasma sheet as shown in Figure 16.

From our earlier discussions, it is clear that reconnection involves an electric field at a separator. If the electric field arises as an inherent part of an instability, e.g., in an unstable linear eigenmode of the system, rather than being imposed from external boundary conditions, the process is called *spontaneous reconnection.*

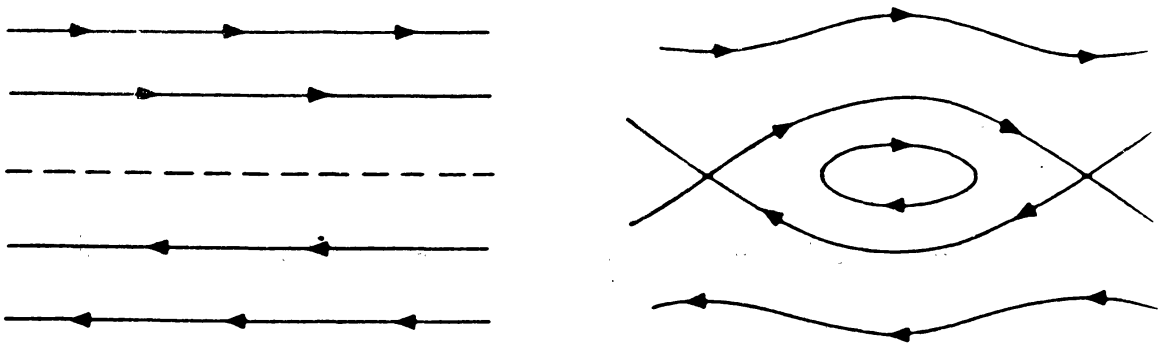

Figure 16. Magnetic topology resulting from the excitation of tearing mode instability.

Tearing mode instabilities have been studied extensively in the context of laboratory plasmas such as Tokamaks and field reversed configuration as well as in space plasmas such as in the earth's magnetosphere and the solar atmosphere. In the earth's magnetosphere, the tearing instabilities have been invoked as a possible mechanism for generating flux transfer events (FTE) and for the onset of substorms Lakhina (1992a, b). Tearing modes require some kind of dissipation in the system for their excitation. When the dissipation is due to the Coulomb collisions, we have *resistive tearing* modes. On the other hand when the dissipation is caused by turbulence or by inertia effect such as by a Landau type resonance, the modes are called *collisionless tearing* modes. The tearing mode consists of the growth of a magnetic island configuration (see Figure 16). The tearing mode affects an increase in the island size and leads the plasma to a state of lower magnetic energy. The time scale for the tearing modes is a hybrid of the MHD time scale t_A and the resistive time scale t_r, as defined below. Excellent accounts of tearing modes can be found in the articles by White (1983) and Galeev (1984). We shall discuss here the resistive tearing modes discovered by Furth, Killeen and Rosenbluth (1963).

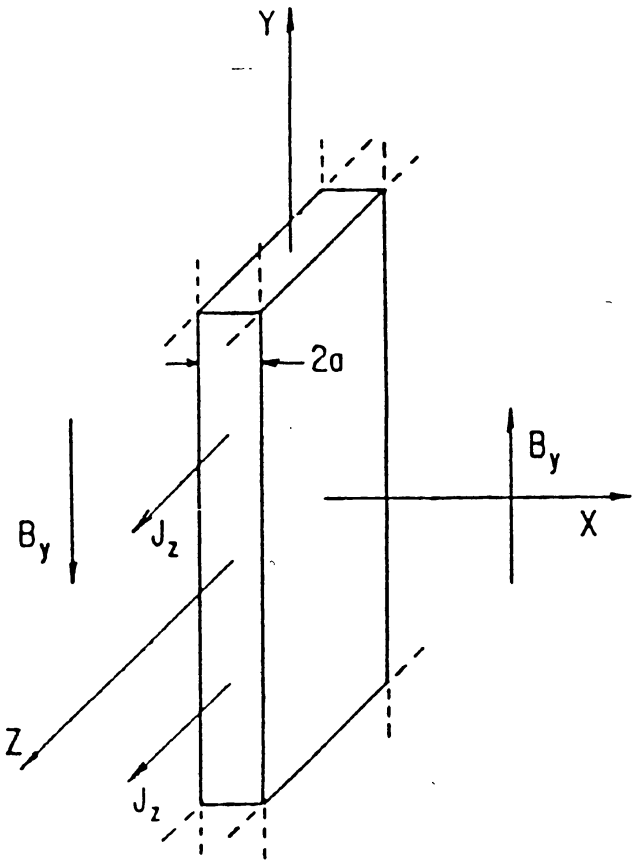

Figure 17. Schematics of the equilibrium current sheet configuration in slab geometry. The current density J_z flows along an external field B_z, generating a self-consistent but much weaker magnetic field $B_y(x)$.

4.1. Resistive tearing mode instability

Let us consider a slab of current with a current density, J_z, and width a, uniform in y - z plane, moving along a large magnetic field B_{0z}. A self consistent magnetic field $B_{0y}(x)$, where $B_{0y}(x) \ll B_{0z}$, is produced which reverses its direction across the current sheet (i.e.,$B_{0y}(0) = 0$) as shown in Figure 17. Hence, we can write the equilibrium sheared field as

$$\mathbf{B}_0(x) = B_{0y}(x)\,\hat{y} + B_{0z}(x)\,\hat{z}. \tag{26}$$

The resistive tearing instability is described by MHD equations which can be cast into the form:

$$\rho\frac{d\mathbf{v}}{dt} = -\nabla p + \frac{1}{\mu_0}(\nabla \times \mathbf{B}) \times \mathbf{B}, \tag{27}$$

$$\frac{d\mathbf{B}}{dt} = \frac{\eta}{\mu_0}\nabla^2\mathbf{B} + \nabla \times (\mathbf{v} \times \mathbf{B}), \tag{28}$$

$$\nabla \cdot \mathbf{B} = \mathbf{0}; \ \nabla \cdot \mathbf{v} = \mathbf{0}. \tag{29}$$

We shall now consider the linear problem. We denote perturbed quantities by the subscript 1, and write them as follows:

$$f_1(\mathbf{x}, t) = f_1(x) \exp(ik\, y + \gamma). \tag{30}$$

Then, the linearized Eqs.(27)-(29), can be reduced to the form:

$$\psi_1(x) = F(x)\phi_1(x) + \frac{1}{\gamma t_r}\left[\psi_1''(x) - k^2\psi_1(x)\right], \tag{31}$$

and

$$-\gamma^2 t_A^2[\phi_1''(x) - k^2\phi_1(x)] = F(x)[\psi_1''(x) - k^2\psi_1(x)] - F''(x)\psi_1(x), \tag{32}$$

where the primes denote the derivative with respect to x which is normalized with a (i.e., $x = x/a$), and $t_r = a^2/\eta$, $t_A = \mu_0^{1/2}\rho^{1/2}/kB_{0y}$ are the characteristic resistive and Alfvén time scales, and $F(x) = \mathbf{k} \cdot \mathbf{B}_0/k\, B_0$. Also, k is normalized with a, i.e., $k = k\, a$. Furthermore, the flux function $\psi_1(x)$ and the stream functions $\phi_1(x)$ are defined by the following relations:

$$\begin{aligned} \mathbf{B}_1 &= \nabla\psi_1 \times \hat{z}, \\ \mathbf{v}_1 &= \nabla\phi_1 \times \hat{z}, \end{aligned} \tag{33}$$

Equations (31) and (32) are to be solved with the boundary conditions that $\phi_1(x) = \psi_1(x) = 0$ at $x = \pm\infty$.

For ideal MHD, i.e., for $\eta = 0$, one can show that the system is stable. Finite resistivity allows the tearing instability to relax the system to a lower magnetic energy state. The second term on the right of Eq.(31) is generally of the order of $1/S$, where $S = t_r/t_A \gg 1$ is the magnetic Reynolds number, and therefore negligible. However, at a value of x at which $\mathbf{k} \cdot \mathbf{B}_0$ is zero (i.e, $F = 0$), this term cannot be neglected. Thus, we find that the resistivity is important only in a narrow layer of width $\Delta \ll a$, called the resistive layer (or diffusion region or inner region), centered around $x = 0$, where $\mathbf{k} \cdot \mathbf{B}_0 = 0$.

Outside the diffusion region, the ideal MHD holds good and one can put $\eta = 0$. Thus the implication of a large magnetic Reynolds number is not that resistivity is negligible but that this resistive layer is very narrow compared to the system length The method of the tearing mode analysis is to find the solutions of Eqs.(31) and (32) in the outer region (or external region) defined by $|x| > \Delta$, where resistivity is negligible, and in the inner region ($|x| < \Delta$), and finally match the two solutions to obtain the dispersion relation.

Let us first examine the outer region where η is negligible. Assuming that scale lengths for the solution are of the order of the shear length, and using $\gamma t_A \ll 1$, we get from Eqs.(31) and (32) the following equations,

$$\psi_1(x) = F(x)\,\phi_1(x); \ \ F(x)\,[\psi_1''(x) - k^2\psi_1(x)] = F''(x)\psi_1(x). \tag{34}$$

We consider a particular profile for $F(x)$ as :

$$F(x) = \tanh(x) \tag{35}$$

which describes the Harris sheet magnetic field profile. The solution for ψ_1, satisfying the boundary conditions $\psi_1 = 0$ at $x = \pm\infty$, can be written as

$$\psi_1(x) = (1 \pm \tanh x\,/k)\exp(\mp k\,x), \tag{36}$$

where the upper (lower) sign corresponds to x positive (negative). The function $\psi_1(x)$ has a discontinuous derivative at $x = 0$, which is given by

$$\Delta'_{outer} = \frac{[\psi_1(0_+) - \psi_1(0_-)]}{\psi_1(0)} = \frac{2(1-k^2)}{k}. \tag{37}$$

Note that $\Delta'_{outer} > 0$ for $k < 1$, i.e, when the shear length is short compared with the wavelength of the mode.

Now, the full resistive equations must be solved in the inner region. Since the inner region width is small i.e., $\Delta/a \ll 1$, $F(x) \simeq x$ within the tearing layer. The nature of the outer solution (cf. Eq.(36)) suggests that within the tearing layer $\psi_1(x)$ is approximatey constant although, of course, $\psi_1'(x)$ must be changing. Physically this would mean that the perturbed flux can readily diffuse across the thin resistive layer during the growth time γ^{-1} of the mode so that $\psi_1(x)$ remains nearly constant in the resistive region. Therefore $\psi_1(x)$ can be approximated by $\psi_1(0)$ on the left hand side of Eq.(31). This is the widely invoked "*constant* ψ " approximation[23]. Also since $\Delta/a \ll 1$, one can take $\psi_1'' \gg k^2\psi_1$, $\phi_1'' \gg k^2\phi_1$, then from the solution of Eqs.(31)-(32) one can get the jump in the derivative of ψ_1 in the inner region,

$$\Delta'_{inner} = \frac{1}{\psi_1(0)}\int_{-\infty}^{\infty} dx\,\psi_1''(x) = \gamma^{5/4} t_r^{3/4} t_A^{1/2} \frac{\pi\Gamma(3/4)}{\Gamma(1/4)}. \tag{38}$$

Now matching Δ'_{inner} to the jump in the outer solution (given by Eq.(37)), we get the growth rate of the resistive tearing mode as

$$\gamma = \left[\frac{2\Gamma(1/4)(1-k^2)}{\pi\Gamma(3/4)k}\right]^{4/5} t_r^{-3/5} t_A^{-2/5}. \tag{39}$$

Clearly the mode is stabilized for $k > 1$. The analysis yields the width of the resistive layer as

$$\Delta = 2(\gamma t_A^2/t_r)^{1/4} = 2(\Delta'_{outer})^{1/5} S^{-2/5} \ll 1. \tag{40}$$

This shows that the width of the resistive layer is indeed small as $S \gg 1$. Further, note that a parallel electric field $E_z = \gamma\psi_1/c$ would be produced in the resistive

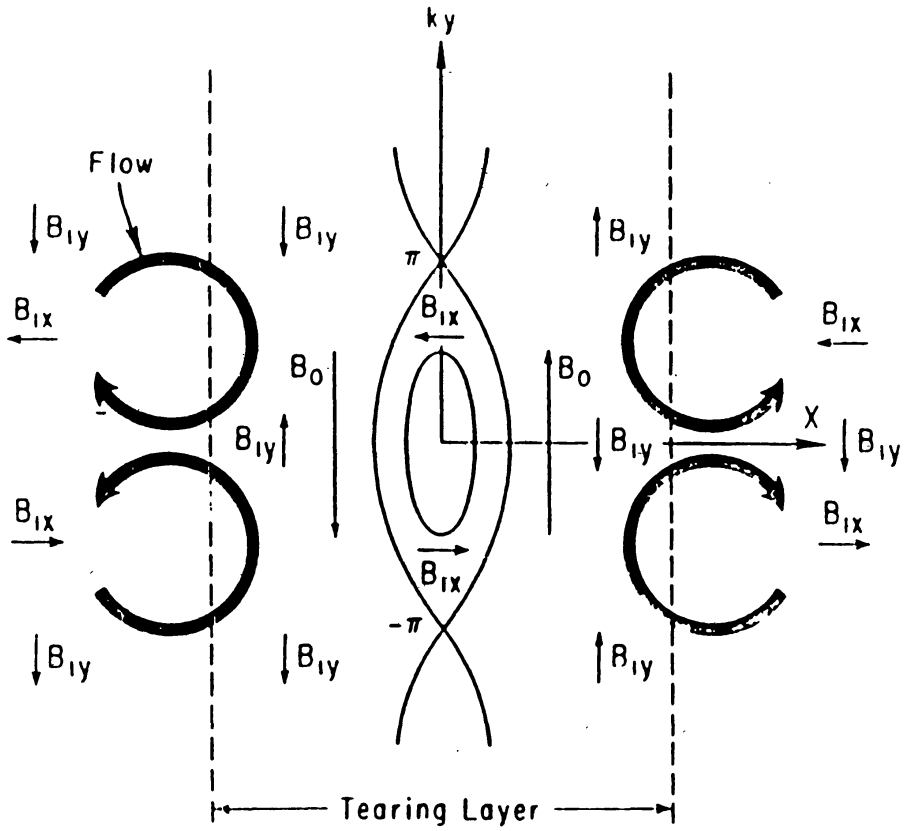

Figure 18. The first- order fields and flow patterns associated with excitation of the tearing mode instability.

layer. First-order fields and flow velocities produced during excitation of tearing modes are shown in Figure 18.

4.2. Recent Developments

Tearing modes have been studied in two dimensional configuration (Lembege and Pellat, 1982; Schindler, 1974; Galeev , 1984), including the effects of shear flow (Lakhina and Schindler, 1983, 1988; Chen and Morrison, 1990), temperature anisotropy (Chen and Palmadesso, 1984), chaotization of the electron orbits (Büchner and Zelenyi, 1987), and coalescence of magnetic islands (Richard et al., 1989).

The driven reconnection, where the perturbations at the boundary induce magnetic reconnection, has been investigated in one dimensional magnetotail configurations by Zelenyi and Kuznetsova (1984) and by Horton and Tajima (1984). Liu and Hu (1988) have shown that flow vortex produced by Kelvin-Helmholtz (K-H) instability can cause magnetic reconnection. Uberoi et al. (1996) suggested surface wave induced magnetic reconnection model. In this model, surface waves,

having wavelengths larger than the thickness of a neutral layer that separates two distinct plasmas, can excite tearing mode instability. Uberoi et al. (1996) find that magnetic reconnection occurs on the tearing time scale. A kinetic theory of driven reconnection for the Earth's magnetotail, which is essentially a two dimensional configuration, has been developed by Lakhina (1992b). It is found that the driven reconnection can occur in two forms, namely the exponential type and the bursty type. The maximum rate of reconnection for the exponential type driven reconnection can be equal to the ion tearing mode growth rate. The bursty type reconnection is short lived, but it occurs at a much faster rate.

Recently, numerical magnetohydrodynamic (MHD) simulation of the evolution of unstable tearing modes has been extensively carried out by many authors, notably among them are Hautz and Scholar (1987), Birn and Hones (1981), Birn and Hesse (1991), and Ogino et al. (1990). Hybrid simulations with electron inertia (Shay et al., 1999) have shown that magnetic reconnection remains Alfvénic in a collisionless system even as the macroscopic scale length of the system becomes very large. The reconnection rate is found to be a universal constant corresponding to an inflow velocity toward the X-line of around 0.1 V_A. Particle simulations (Zwingmann et al., 1990; Ogino et al., 1990) have shown that in three-dimensions, the tearing modes are found to generate plasmoids and flux ropes; an example is shown in Figure 19 taken from Ogino et al. (1990).

Steady state MHD models of reconnection are also being refined by taking into account the asymmetric and shear flows, two fluid effects, and the flux pile- up effects (Gratton et al., 1988; Sonnerup et al., 1990; Biernat et al., 1990). Time-dependent reconnection models have been proposed to explain the occurrence of flux transfer events (FTEs) at the Earth's magnetopause (Russell and Elphic, 1978). Models based on patchy reconnection (Nishida, 1989), a process where the size of the reconnection region has a fairly limited extent, and multiple X-line reconnection (MXR)(Lee and Fu, 1985) , a process in which a magnetic flux tube is reconnected with other tubes at multiple sites, have been proposed to explain the observed features of FTE's. (Lee and Fu, 1986) have carried out an extensive simulation study of magnetic reconnection based on 2-D slab model, some of their results are shown in Figure 20. They showed that the ratio of system length (L_z) to system width (L_x) used in the simulation, the resisitivity, and the flow speed control the evolution of the system to various steady state reconnection configuration. As the ratio L_z/L_x is increased from small to higher values, the system evolves into a steady-state configuration of Petschek-like (cf. Figure 20, panel a) to Sonnerup (cf. Figure 20, panel b) to Sweet-Parker (cf. Figure 20, panel c) to unsteady single-line to a time-dependent multiple X-line reconnection process (cf. Figure 20, panel d).

Of late, there has been a considerable interest in 3-D magnetic reconnection process. When the X-line has a finite extent, 3-D effects become important. In 3-D reconnection, the magnetic topology is complicated, the separatrices and separators cannot be properly defined, and the core magnetic field in a magnetic flux tube can be highly enhanced (Schindler et al., 1988; Hesse and Schindler,

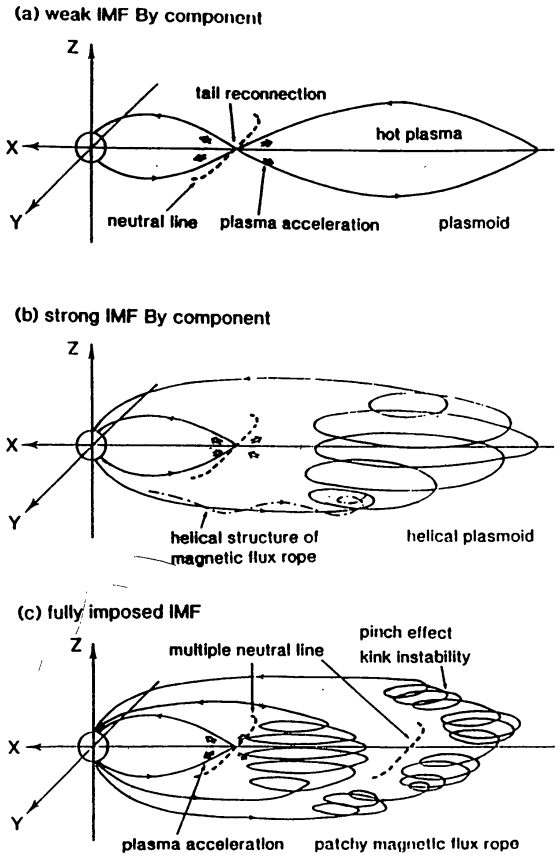

Figure 19. Schematics of the magnetic configuration of plasmoids in the magnetotail: (a) configuration for sunwards IMF polarity (only a small or no B_y component), (b) when IMF has a large B_y component in addition to southward component. In cases (a) and (b) the IMF initially entered the simulation box from the left edge. (c) when the southward and dawnward IMF initially superimposed everywhere in the simulation box (taken from Ogino et al., 1990).

1988; Greene, 1988; Otto et al., 1991; Lee et al., 1993; Ma et al., 1994). Figure 21 shows an example of the patchy multiple X-line reconnection (PMXR) process (Lee et al., 1993). In Figure 21a, two strips of interplanetary (AA' and BB') and magnetospheric magnetic flux (CC' and DD') are shown in a projection onto the magnetopause. The elbow like interlinked flux regions, CA' and BD', are formed when reconnection takes place at two patches as shown in Figure 21b. These newly reconnected regions approach each other due to unbalanced magnetic tensions (cf. Figure 21c), and could further reconnect to form two flux tubes, one (i.e., CD') being connected only to the geomagnetic field and the other (i.e., BA') only to the IMF as shown in Figure 21d.. Reconnection at three appropriate locations can also lead to similar topological results as shown in Figure 21e. Figure 21f shows a case where reconnection could take place at four locations, leading to the formation of four open flux tubes.

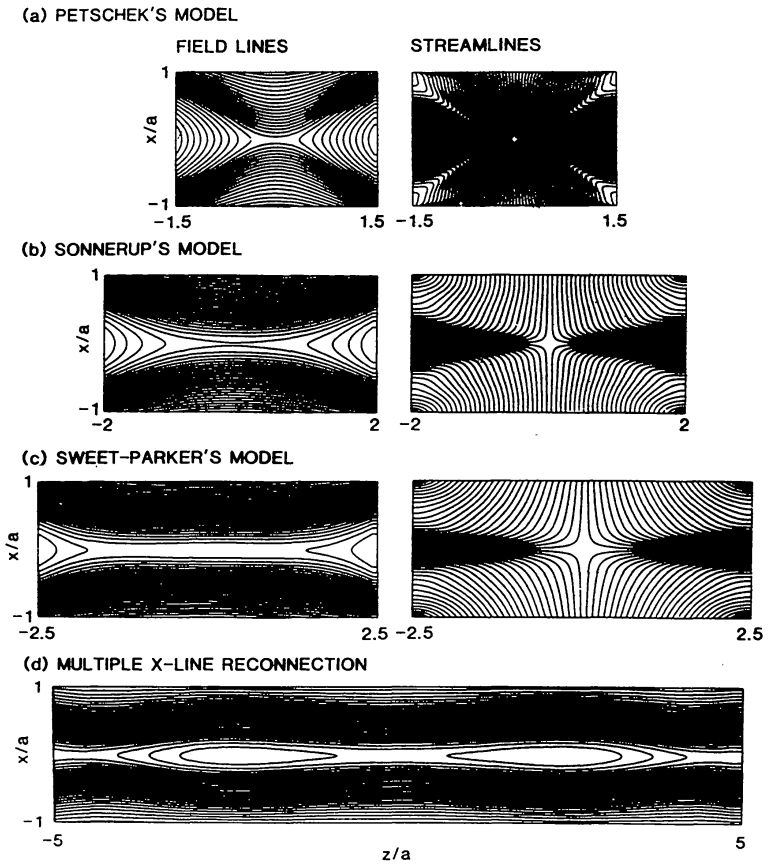

Figure 20. Magnetic field lines and streamlines in (a), (b) and (c) are for a steady-state single x-line reconnection, and (d) for time-dependent x-line reconnection [after *Lee and Fu*, 1986].

4.3. Reconnection Signatures

Magnetic field line reconnection is a process that converts magnetic field energy into kinetic energy of plasma. Two main signatures of the reconnection are the plasma jets flowing out of the diffusion region and the change in the magnetic field topology. The particles can be directly accelerated by the induced reconnection electric fields along the X-line or parallel electric fields, or by the electric fields of the shocks produced during the reconnection process. In the region near the neutral line, the plasma is Joule heated /accelerated by the strong currents developed during the reconnection. The kinetic energy of the plasma jetting out of the diffusion region itself is $\sim m_i V_A^2/2 = 4.0 \times 10^{-2}\, B^2/n$ erg, where B is in gauss and n in cm^{-3}. In exceptional solar flare cases when B is very high and n is low, a particle can achieve energy as high as 10 MeV/nucleon due to this bulk acceleration alone. On the other hand, the energies gained by the particles by the direct acceleration at the magnetic null line or X-line is found (Speiser, 1965) to be $E = 10^{-6}\, BLV_{in}$ erg, where B, the asymptotic field at the edge of the field reversed region, is expressed in gauss, L, the length of the X-line, in km, and V_{in}

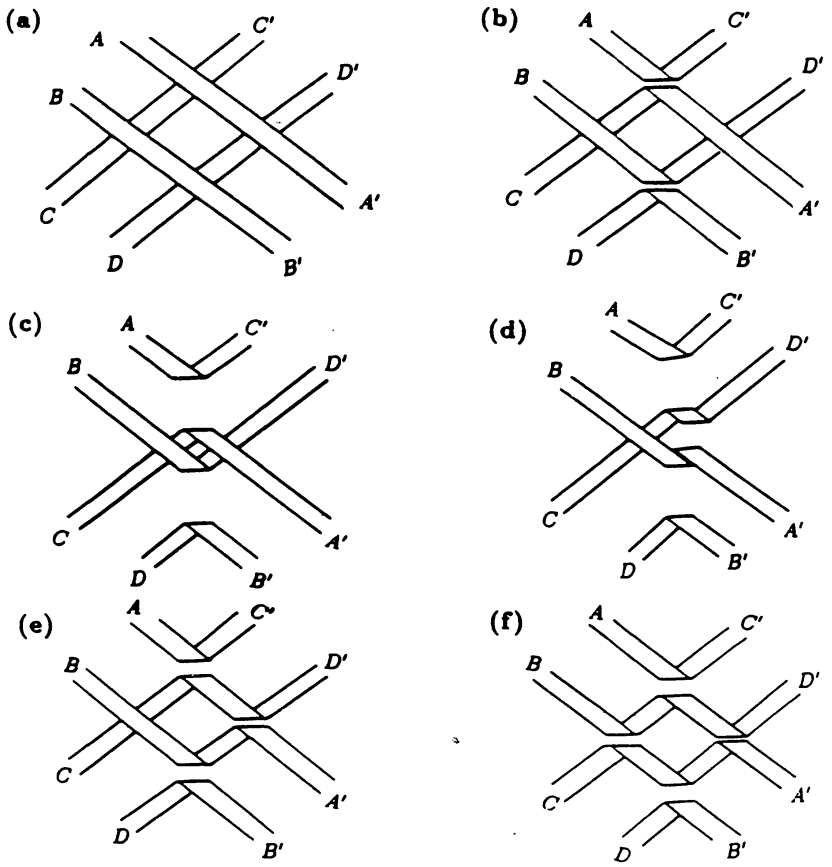

Figure 21. Schematics of reconnection at multiple patches. (a) AA' and BB' are two bundles of magnetosheath field lines and CC' and DD' of magnetospheric fields. (b) Reconnection takes place at two patches. (c) Flux tubes BD' and CA' move towards each other. (d) Reconnection occurs leading to formation of closed flux tubes CD' and BA'. (e) Reconnection at three patches with flux tube AA' having reconnection at two sites. (f) Reconnection at four patches with each flux bundle reconnected at two sites [after *Lee et al.*, 1993].

the inflow speed in km s^{-1}. This mechanism is shown in Figure 22 for the ion motion. The particle enter the neutral sheet region with velocity V_{in}. Outside the field reversal region the particle orbit consists of a gyration in the z - y plane. Since the motion is oscillatory, the average energy gain is zero. Once a particle is inside the field reversed region, it is simply accelerated in the y direction. A Lorentz force in the x direction eV_yB_z now acts on the ion, however, and turns its motion around in the x - y plane (i.e., plane of the current sheet). The ions continue to turn in this plane until they are moving nearly in the x direction, i.e., along the direction of the field just outside the field reversed region. At this point the ions are no longer trapped by magnetic forces with in the current sheet, and they are ejected as a nearly field-aligned beam along the reconnected field lines away from the X-line.

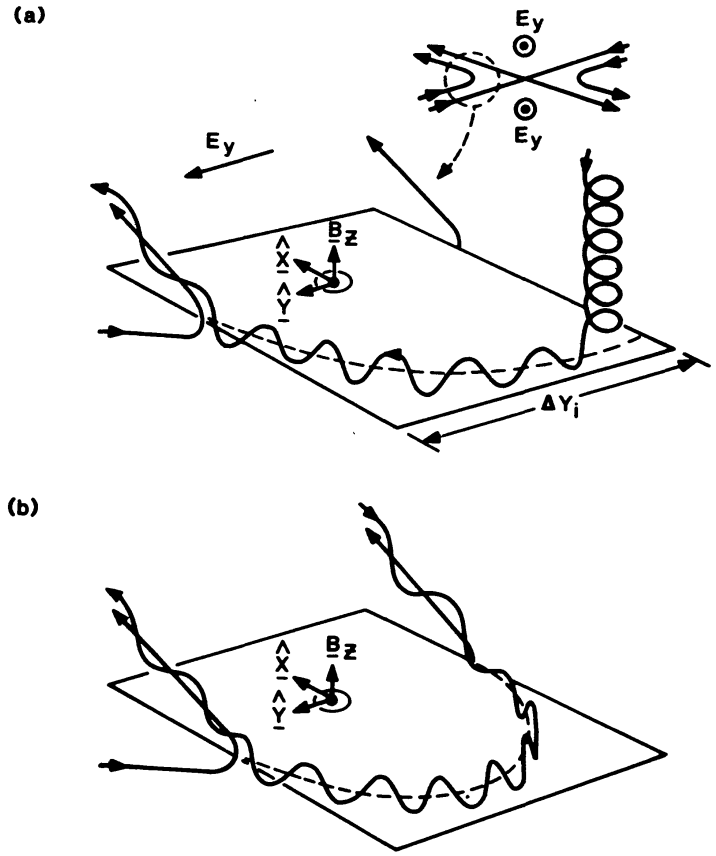

Figure 22. Schematics of ion motion in a current sheet in (a) the neutral line rest frame ($E_y \neq 0$), and (b) the field line rest frame ($E_y = 0$). The latter rest frame is moving with a speed of $V_F = E_y/B_n$ away from the X-line. In the field reversed region near the X-line, the motion is non-adiabatic (Speiser orbits). The ions are accelerated by the reconnection electric field in this region

5. Disruption of Forced Current Sheets

Current sheets play a crucial role in many astrophysical situations requiring intense dissipation of magnetic energy into thermal and flow energy of the plasma, and this conversion is achieved by magnetic reconnection. Current sheets can occur in almost all cosmic plasmas. For example, the current sheets in the bipolar magnetic regions on the sun and other stars could arise simply because of the continual mixing and swirling of the foot points of the magnetic field line in the subphotospheric/photospheric convection. The current sheets are also expected to be created in magnetic field of galaxies and within clusters of galaxies.

The disruption of current sheets releases the excess stored magnetic energy via magnetic reconnection process and consequently the plasma system relaxes to a new equilibrium configuration with less free energy than before. The disruption of current sheets could provide the necessary heat source responsible for the X-

ray corona and the X- ray emission from almost all stars. Parker (1988) has suggested that the X-ray corona and much of the region of a steller flare could be due to a cloud of small reconnection events (*nanoflares*) in the ambient current sheets. Some other phenomena associated with the disruption of current sheets are the loop prominences (Kopp and Pneuman, 1976), coronal mass ejections (Pneuman, 1980), solar flares (Howard and Svestka, 1977; Priest, 1981; Tajima et al., 1985; Sturrock et al., 1986; Svestka et al., 1992), microwave solar bursts (Kundu, 1985), magnetosphere substorms (Coppi et al., 1966; Schindler, 1974; Hones, 1979, and comet- tail disconnection events.

It is customary to treat the current sheets as tangential discontinuities without any flow. However, the theoretical analysis and simulation studies show that when topologically different parts of a magnetic configuration are pushed together either due to convection, or slowly changing boundary conditions or because of vortex flows induced by a macroscopic instability, a thin forced current sheet may form in the center of the ambient current sheet (Burkhart et al., 1992). The forced current sheets carry strong currents, have a thickness of the order of an ion Larmor radius, and are characterized by a finite B_n, the component of the magnetic field normal to the current sheet, as has been observed during the growth phase of the substorms in the Earth's magnetotail (Mitchell et al., 1990).

Figure 23 shows schematics of a thin current sheet embedded in the magnetotail as observed during growth phase of a substorm. The thin current sheet is characterised by a half-thickness, a, which is much smaller than the half thickness of the plasma sheet L. The strong current within this embedded sheet in not due to diamagnetic drift (i.e., the apparent drift due to the difference in the plasma populations on the adjacent field lines); rather, it is due to the acceleration of "Speiser like" ions tractories by a dawn to dusk electric field, E_y. Lakhina (1993a,b) and Lakhina and Tsurutani (1998b) have studied spontaneous reconnection in such a forced current sheet. Under some circumstances, such current sheets can disrupt releasing stored magnetic energy as required for substorms, solar flares, and coronal transients.

6. Solar flares and reconnection

The basic problem of solar flare theory is to explain the initial explosive energy release of as much as 10^{32} ergs in a short time- scale of a few hundred seconds (Svestka et al., 1992). The explosive phase of the solar flare is manifested in the generation of a hot ($\approx 10^7$ K) X-ray emitting plasma in the lower corona. The details of the plasma heating, which appears to be common to all flares, as well as mechanism(s) for injection of particles are still not well understood. Not only is the hot plasma a main source for the X-ray emission, it may well provide the energy for EUV and Hα flares (Sturrock, 1973; Craig, 1981). The conventional view is that the annihilation of coronal magnetic fields via magnetic reconnection process provides the necessary flare energy, but a complete flare theory which can

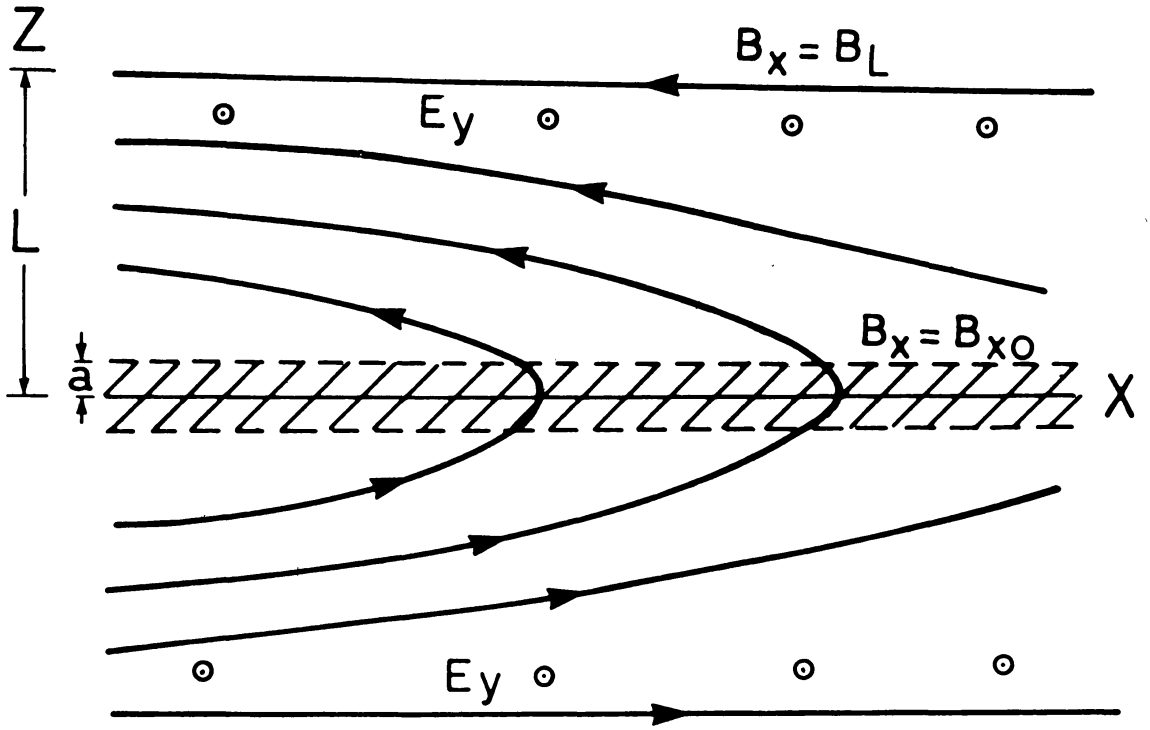

Figure 23. Schematics of the two dimensional configuration of The earth's plasma sheet with an embedded forced current sheet at the center. The plasma sheet has a characteristic dimension of $2L$ and the forced current sheet (hatched region) has a half thickness of a. The x-component of the magnetic field has a value B_{xo} just outside the boundary of the inner current sheet (dashed horizontal line), and a value B_L in the lobe region. A uniform dawn to dusk electric field E_y is imposed on the plasma sheet. The forced current sheet has a finite B_n. (taken from *Lakhina* [1993a]).

also predict radiation spectra for comparison with observational data in X-ray, EUV, optical and radio wavebands is not available. Figure 24 shows a schematic profile of the flare intensity in several wave lengths. It is found that long duration event (LDE) flares, associated with soft X-ray emission, typically last more than an hour, whereas the impulsive flares are short lived lasting for much less than an hour. The latter are characterized by the impulsive hard X-ray emission.

The solar corona is composed of a complex network of individual loop-like structures as is seen in high resolution X-ray images of the quiet and active Sun using satellite and rocket-borne instruments. Only in the coronal holes, which are the regions of open field lines with low pressure and relatively low emissivity, such loops appear to be absent. Usually, small, low-lying loops with enhanced temperature and density ($T > 3 \times 10^6$ K and $n_e > 10^9$ cm^{-3}) form the nucleus of the flare active-region. These are overlaid by longer broader, but more diffused

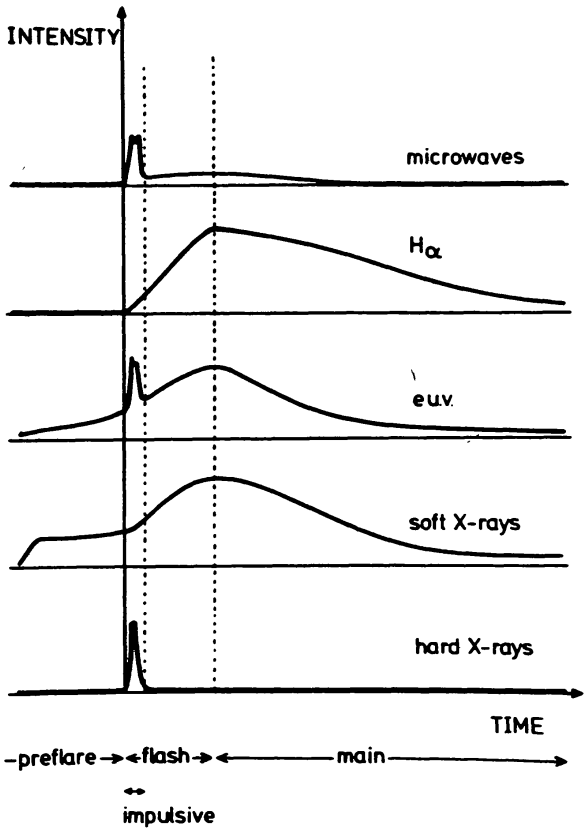

Figure 24. Schematics of the solar flare intensity in several wavelengths. There is a lot of variation in the duration and complexity of various phases, but for a large event the preflare phase lasts typically 10 minutes, the impulsive phase 1 minute, the flash phase 5 minutes and the main phase 1 hour.

structures, while still longer loops may interconnect individual active regions. It appears that all loops can be excited either directly by the initial magnetic energy release or indirectly by some secondary flare disturbance, but the smaller loops have a greater tendency to flare. The information on the thermal structure of the active-region loops is derived mainly from X-ray and EUV spectral data. For an isothermal source, the spectrum is determined by just two parameters, the temperature T and the emission measure $\int n_e^2 dV$, where V is the volume of the source emitting X-rays.

6.1. Solar Flare Models

Several models, involving magnetic reconnection in some form or the other, have been proposed for solar flares. Indeed, it is likely that a number of different mechanisms are operating to produce flares of different types. We will here discuss briefly only a few of them.

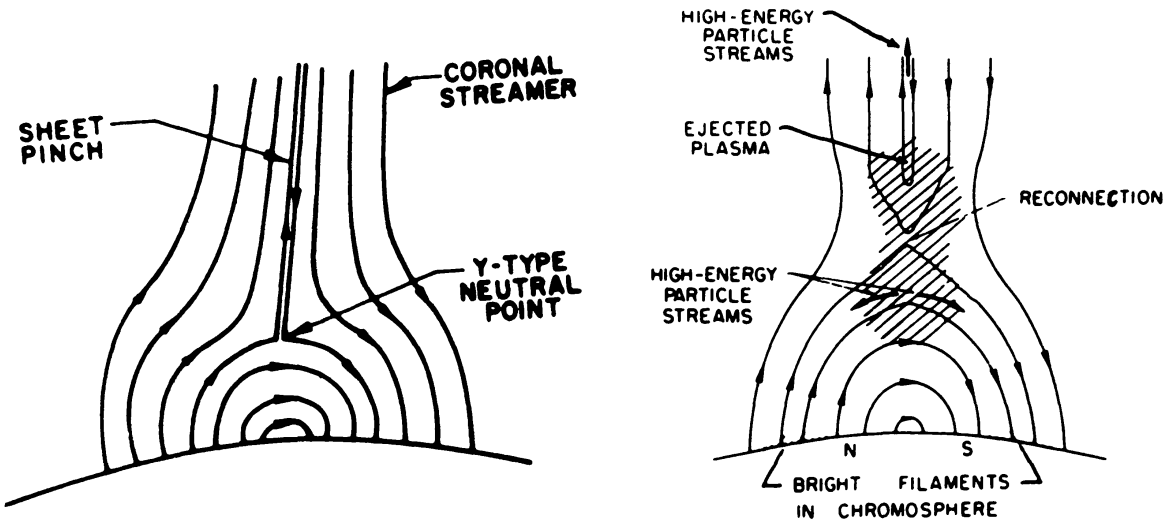

Figure 25. Sturrock's solar flare model. (taken from *Sturrock*, 1974).

6.2. Sturrock's Model

Figure 25 shows the basic features of the solar flare model proposed by Sturrock (1974). It has a helmet-streamer-like magnetic field configuration. The impulsive phase of the flare is due to a tearing mode instability which generates a strong electric field in the open current sheet. This leads to fast electrons, those escaping along the current sheet produce type III radio bursts, while others travelling down to the chromosphere produce hard X-ray burst. During the flash phase, reconnection continues due to Petschek's mechanism and two ribbons of emission are formed when heat and energetic particles reach the chromosphere. This model has been refined by several workers (Charmichael, 1964; Hirayama, 1974; Kopp and Pneuman, 1976), and is also commonly known as Carmichael-Sturrock-Hirayama-Kopp-Pneuman (CSHKP) model.

6.3. Emerging Flux Model

High-resolution observations have shown that flares tend to occur after the emergence of new flux from the photosphere. Figure 26 shows the emerging flux model

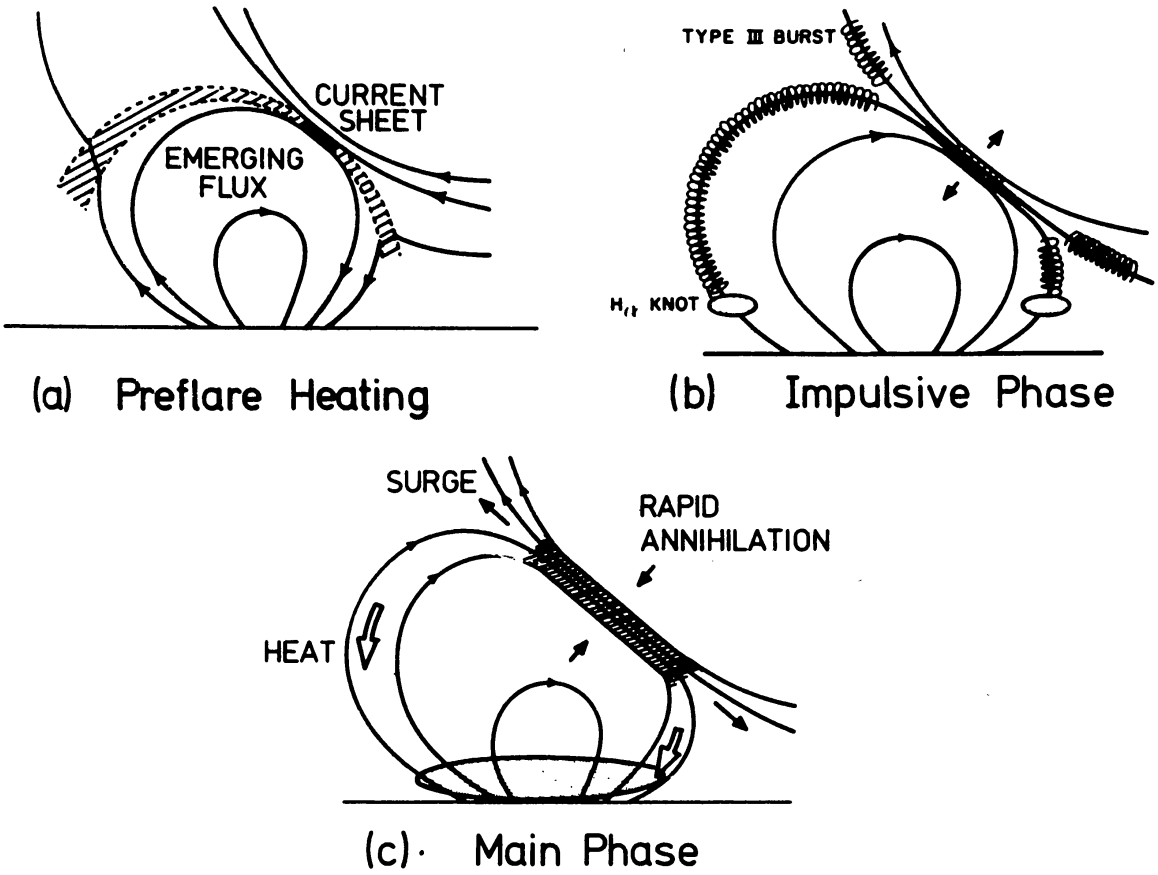

Figure 26. The emerging flux model for a simple-loop flare. (a) *Pre-flare phase.* The emerging flux reconnects with the overlying fields. Shock waves (dashed lines) radiate from a small current sheet and heat the plasma as it passes through them into the shaded region. (b) *Impulsive phase.* The onset of turbulence in the current sheet, after it reaches a critical height, causes a rapid expansion. The resulting electric field accelerates particles, which then escape along the field lines and produce an impulsive microwave burst. Those that move downwards give rise to hard X-rays by collisional excitation (and possibly H_α knots). (c) *Flash and Main phase.* The current sheet reaches a new steady state, after undergoing reconnection due to the turbulent resistivity. The reconnection region is much bigger than before and both heat and particles are conducted down to the lower chromosphere where they produce the H_α flare. (after *Heyvaert et al.*, 1977).

for a small flare (a simple-loop flare) as proposed by Heyvaert et al. (1977). During the preflare phase, steady reconnection occurs in the current sheet formed between the new and the old flux. At some critical height, plasma instabilities are excited once the current density exceeds the threshold value. As a result the current sheet heats up, seeking a new equilibrium state. This triggers the flare leading to impulsive phase in which particles are accelerated to high velocities by the resulting electric fields. Finally, in the main phase, the system reaches a new steady state of magnetic field reconnection where the current sheet is marginally turbulent.

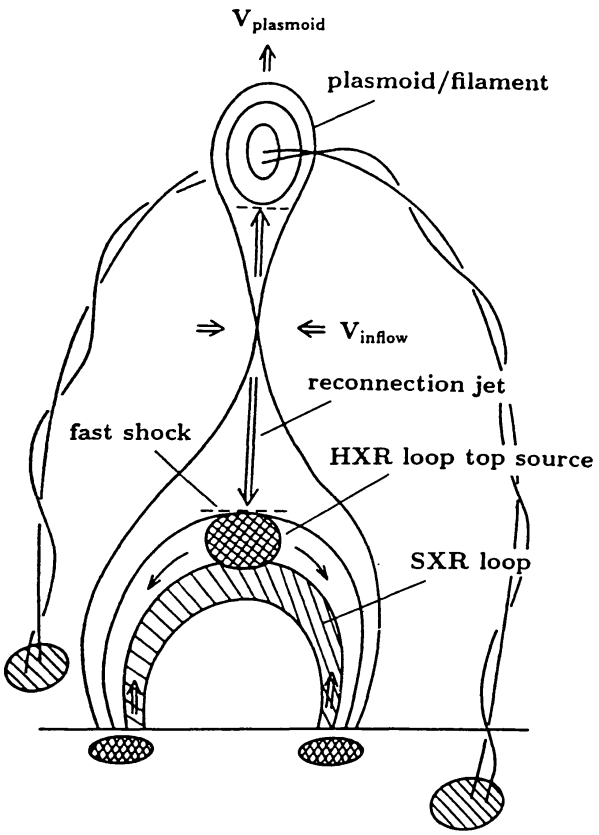

Figure 27. A unified model of a flare: a plasmoid-induced-reconnection model (taken from *Shibata*, 1996).

6.4. Plasmoid-Induced Reconnection Model

On the basis of observations related to X-ray plasmoid ejection before the impulsive phase of the solar flare, Shibata (1996) has proposed the plasmoid-induced-reconnection model by extending the classical CSHKP model, as shown in Figure 27. In this model, plasmoid ejection plays a crucial role to trigger fast reconnection. When the plasmoid suddenly rises with velociy $V_{plasmoid}$, it will lead to the plasma inflow V_{in} toward the X-point to compensate the mass ejected by the plasmoid. Assuming that the density does not change significantly during the eruption, one can write

$$V_{in} \sim V_{plasmoid}\, L_{plasmoid}/L_{in},$$

where $L_{plasmoid}$ and L_{in} are the typical sizes of the plasmoid and the inflow region, respectively. The impulsive phase is identified with the condition $L_{plasmoid} \sim L_{in}$, i.e., when,

$$V_{in} \sim V_{plasmoid} \sim 50 - 400 \mathrm{kms}^{-1}.$$

Since the reconnection rate is determined by the inflow speed, the ultimate origin of fast reconnection in this model is the fast ejection of a plasmoid. After the impulsive phase, L_{in} becomes larger than $L_{plasmoid}$ because the distance between the plasmoid and the X-point increases, and hence the inflow speed V_{in} would decrease, leading to slow reconnection which corresponds to the decay or the late phase. Since the electric field $E \sim V_{in}B/c$ near the X-point is the largest during the impulsive phase, the model naturally explains acceleration of higher energy electrons in the impulsive phase than in the decay phase.

6.5. Simulation Models

On the basis of numerical simulation model, Antiochos and DeVore (1999) have emphasized that magnetic reconnection in the corona must have an "off-on" nature in order to produce explosive eruptions. Yokoyama and Shibata (1995, 1996) have developed magnetic reconnection model of X-ray jets using 2.5D MHD numerical simulations; some results are shown in Figure 28. In this model, magnetic reconnection occurs in the current sheet between emerging flux and overlying coronal fields as in the classical emerging flux model (Heyvaert et al., 1977; Forbes and Priest, 1984). Interesting features of this model are:
1) The reconnection starts with the formation of magnetic islands (i.e., plasmoids). These islands coalesce with each other and finally are ejected out of the current sheet. The largest energy release occurs after the ejection of the biggest island,.
2) The reconnection jets from the X-point soon collide with the ambient field to form fast shocks. The global jets emanate from the high pressure region just behind the fast shock, and propagate along the reconnected field line, as shown in Figure 29. This suggests that observed X-ray jets are not the reconnection jet itself, but hot jets accelerated by the enhanced gas pressure behind the fast shocks.
3) The emission measure is the smallest at the X-point, since the volume of the X-point is very small (Yokoyama and Shibata, 1996). Thus the X-point is not bright and hence is not easy to detect. This may be the reason why there is a gap between a jet and the brightest part of a footpoint flare.

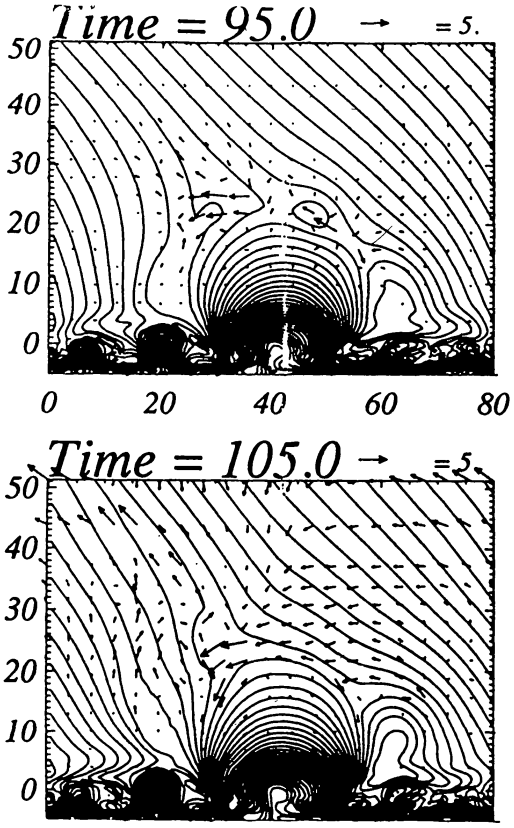

Figure 28. Simulation model of the solar flare based on emerging flux reconnection. An interesting feature of this model is that plasmoids (magnetic islands) are created repeatedly in the current sheet (taken from *Yokoyama and Shibata*, 1995).

6.6. Observational Support for Reconnection in Solar Flares

Recent observations on rapidly time variable phenomena on the Sun such as jets, and impulsive flares provide strong support to the idea of magnetic reconnection taking place during such events. Most of the evidence has come from the two imagers, namely the soft X-ray telescope (SXT) and hard X-ray telescope (HXT) on board Yohkoh satellite (Kosugi et al., 1991; Ogawara et al., 1991). As the soft X-ray emission originates from hot and dense plasma confined by magnetic fields, the SXT is ideal for studying the coronal magnetic-field topology and its changes during a flare. On the other hand, hard X-rays are emitted via electron-ion Bremsstrahlung from energetic electrons produced during the impulsive phase. Thus combined with SXT, HXT has the capability to locate the particle acceleration site and/or the particle precipitation site in the evolving magnetic field configurations. Therefore, Yohkoh is well equipped to examine the key problem of solar flares, i.e., the magnetic field topology and the energy release involving possibly the reconnection process.

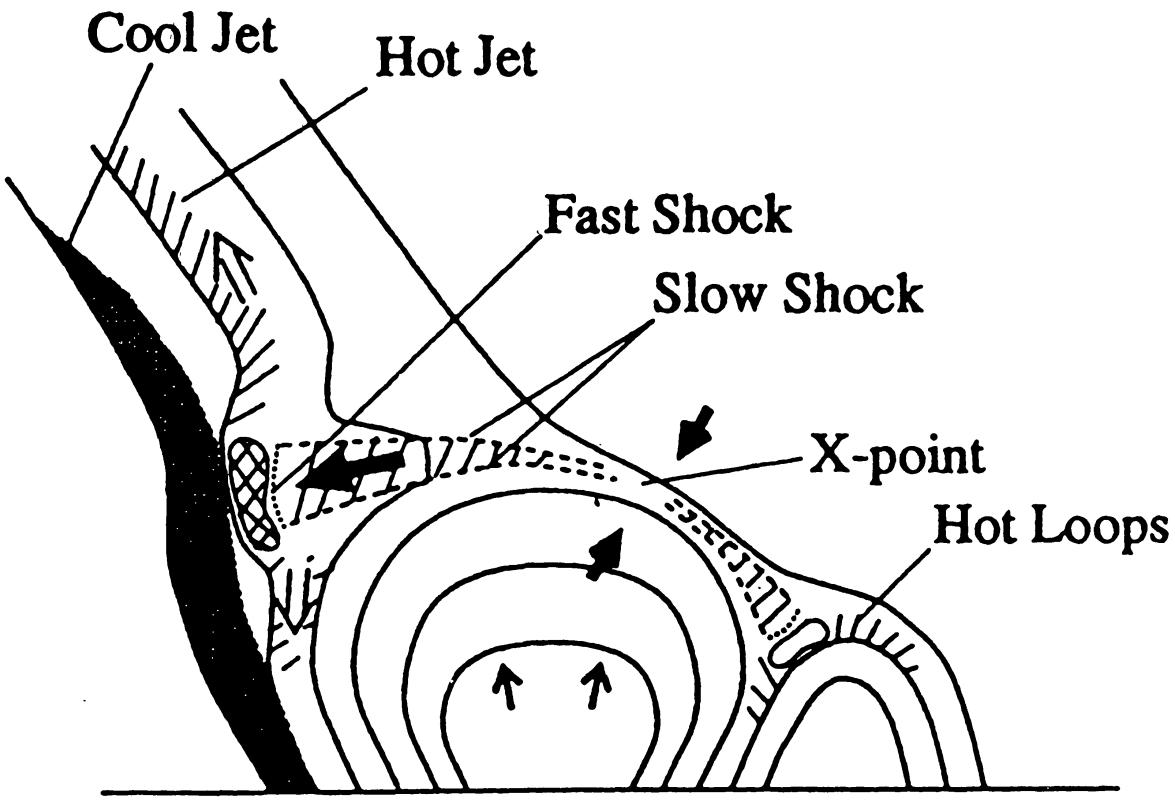

Figure 29. Schematic illustration of physical processes found from numerical simulation of magnetic reconnection associated with emerging flux (taken from *Yokoyama and Shibata*, 1996).

6.6.1. Observation of cusp-shaped loop structure

Figure 30 shows the soft X-ray image of LDE flare, which occurred on February 21, 1992, taken by SXT on Yohkoh (Tsuneta et al., 1992; Tsuneta, 1996). This figure shows a *cusp-shaped loop* structure. It is observed that many LDE flares show such *cusp-shaped loop* structures which are quite similar to magnetic field configuration predicted by the classical magnetic reconnection model (Sturrock, 1974). The outer boundary portion of the cusp-shaped loops has higher temperature than the portion inside the loop, and that the whole loop increases its height and foot-point separation with time. Furhter, the plasmoid ejections have often been observed in the rise phase of LDE flares (Hudson, 1994). Since the energy release rate and other physical quantities are consistent with the prediction of the reconnection model, all these observations strongly support the reconnection model of the LDE flares (Tsuneta, 1996).

Figure 30. Long duration event (LDE) flare on 21 February 1992 observed with soft X-ray telescope (SXT) (taken from *Tsuneta et al.*, 1992).

6.6.2. Loop-Top impulsive hard X-ray source

The soft X-ray images of normal impulsive flares usually show only a bright single-loop, as already known from the Skylab observations. So, it was first thought that the mechanism by which impulsive flares are created could be different from that of LDE flares, i.e., some mechanism other than reconnection may be responsible for the impulsive flares.

Masuda et al. (1995) studied the impulsive flares by carefully co-aligning the SXT and the HXT images of some impulsive compact loop flares observed at the limb. They found that there is an impulsive hard X-ray source above the soft X-ray loop, in addition to the footpoint impulsive double hard X-ray sources. Figure 31 shows their results for the January 13, 1992 flare (Masuda et al., 1995). Since the impulsive hard X-ray sources are produced by high energy electrons which are closely related to the main energy release mechanism. This means that the main energy release occurred above (i.e., outside) the soft X-ray loop. Masuda et al. (1995) postulated that the basic magnetic field configuration for the impulsive flares is quite similar to that of LDE flares as shown in Figure 32. The high speed

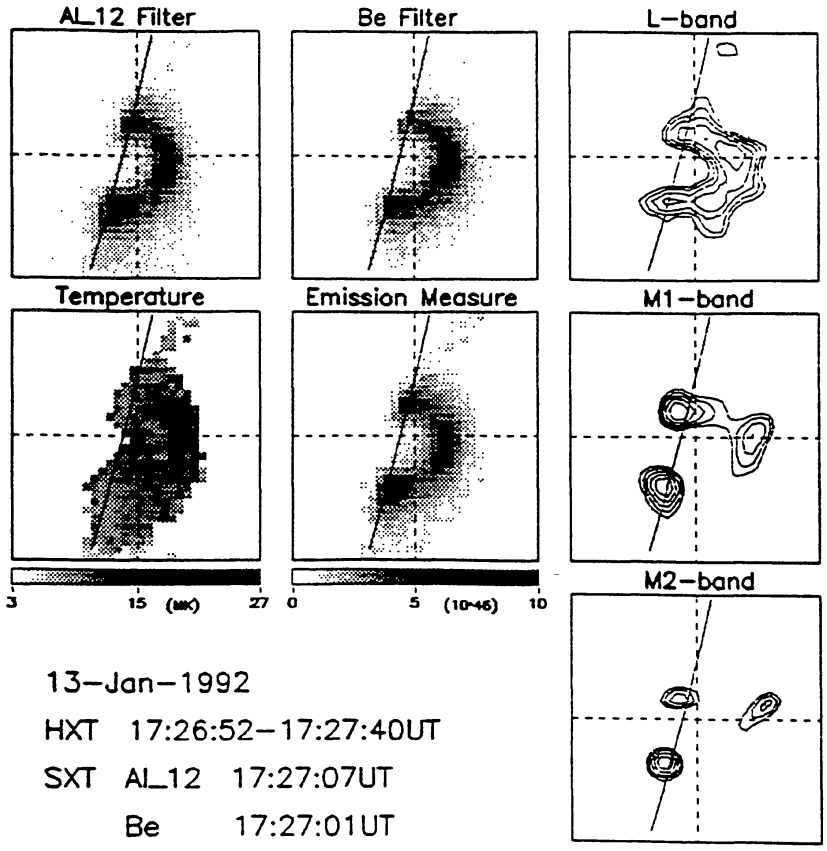

Figure 31. Hard X-ray images (contours) and soft X-ray images (contours) for the 1992 January 13 flare. Temperature and emission measure maps deduced from a pair of SXT images with different X-ray filters are also shown. HXT images are given for the L-, M1-, and M2-bands from top to bottom. Contour levels are 70.7, 50.0, 35.4, 25.0, and 17.7 % of the peak intensity for each map (taken from *Masuda et al.*, 1995).

jet produced by reconnection collides with the top of the underlying closed loop to form a shock producing a hot region as well as high energy electrons which in turn lead to double hard X-ray emission at the foot-points. The anti-parallel magnetic field lines are supposed to be created in association with a prominence (or a dark filament) eruption, and the rising X-type (or Y-type) reconnection point explains the observed increasing separation of the Hα flare ribbons and the increasing height of the post flare loop with time.

6.6.3. Plasmoid Ejection

If reconnection is the cause of the impulsive compact loop flares as suggested by Masuda et al. (1995), then one should be able to observe the plasmoid ejection high above the loop-top hard X-ray source. Shibata et al. (1995) searched for such plasmoid ejections using SXT in 8 impulsive compact flares observed at

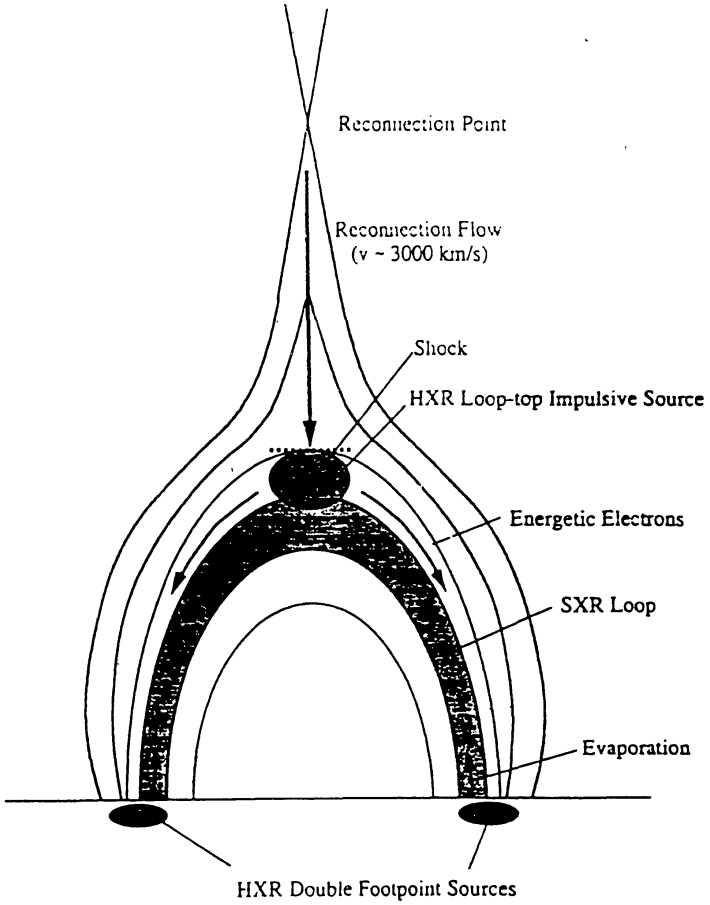

Figure 32. Schematic model for explaining the "loop-top" impulsive hard X-ray source well above the soft X-ray loop. The outflow from the reconnection site in the current sheet with velocities $\geq$ 300 km s^{-1} impinges upon the closed loop and forms a shock, which creates the 2×10^8 K plasma and accelerates electrons. The former is seen as the "loop-top" impulsive source, while the latter streams along the magnetic loops towards the two foot-points, where hard X-rays are emitted via electron-ion Bremsstrahlung. The soft X-ray loop represents previously reconnected magnetic loop filled with material evaporated from the dense chromosphere (taken from *Masuda et al.*, 1995).

the limb. They indeed found that all these flares were associated with X-ray plasmoid ejection. The apparent velocity of these ejections were 50 - 400 km s^{-1}, and their heights were $(4 - 10) \times 10^4$ km. Further, flares with hard X-ray source well above the loop-top show systematically higher plasmoid velocity. The soft X-ray intensity of the plasmoids is very low, typically $10^{-4} - 10^{-2}$ of the bright soft X-ray loop. The plasmoids are found to have various different shapes, e.g., loop-like, blob-like (Ohyama and Shibata, 1997), or jet-like, similar to coronal mass ejections (CMEs) (Burkepile and Cyr, 1993). Ohyama and Shibata (1997) analyzed the temperature distribution of plasmoids, flare loops, and ambient structures, and have noticed that the temperature of plasmoids is $\sim (6 - 13) \times 10^6$ K, less than that of the flare loop, and the overall temperature distribution is consistent with the predictions of the reconnection model. Ohyama and Shibata

(1997) also showed that the kinetic energy of plasmoids is much smaller than the total flare energy. This clearly shows that the plasmoids cannot provide the necessary solar flare energy. However, they could play a role to trigger the main energy release in the impulsive phase as some preflare events show plasmoid ejection (at 10 km s^{-1}) well before the impulsive phase.

7. Magnetospheric substorm and reconnection

7.1. Magnetospheric Substorms

The geospace environment is dominated by disturbances produced directly by the Sun, such as solar flares and coronal mass ejections which are responsible for some large geomagnetic storms or else by disturbances, e.g. substorms, occurring within the magnetosphere that are ultimately caused by the solar wind variations (Gonzalez et al., 1994). A large portion of the energy extracted from the solar wind by the solar wind-magnetosphere (SM) dynamo is stored in the form of excess magnetic flux in the magnetotail region, which, subsequently, is explosively released in the form of energetic particles and strong plasma flows and dissipated in the near-Earth nightside region causing discrete and bright auroras in the polar regions; this phenomenon is called a magnetospheric substorm. During substorm activity, the cross-tail current is disrupted and diverted towards the ionosphere as a field-aligned current. Energetic particle precipitation causes enhanced auroral activity and there is an enhancement in the ring current and westward electrojet current associated with a Pi 2 micropulsation burst and a westward travelling surge. Further, as the magnetospheric convection increases, the plasma sheet tends to move earthward and a part of the plasma sheet is severed from the earth, forming a "plasmoid" that flows out tailwards. Magnetospheric substorms last for about an hour to a few hours. When the substorms occur frequently they can give rise to geomagnetic storms which are characterized by a main phase during which the magnetic field at the Earth's surface is greatly depressed. This is due to strongly intensified ring current formed by the intense fluxes of energetic protons injected during successive substorms. Thus,the magnetospheric substorms represent a global interaction between the solar wind, the magnetosphere and the ionosphere (Kan et al., 1991; Kamide and Kroehl, 1994).

The disturbances due to geomagnetic storms and substorms together are termed as geomagnetic activity. The geomagnetic activity is commonly characterized by changes in the polar electrojets (measurable by the auroral electrojet (AE) index), by the ring current (measurable by the Dst index representing mainly the disturbance in the horizontal component of the geomagnetic field during magnetic storms), and by ionospheric disturbances (monitored by the plasma frequency of the F2 layer (foF2) or by particle precipitation). During

intense geomagnetic storms and substorms, the rate of energy released into the inner magnetosphere can be several times 10^{12} W and the total energy dissipated in the magnetosphere-ionosphere system can be $\sim 10^{22}$ - 10^{23} erg. Therefore, magnetospheric substorms and major geomagnetic storms can produce intense, highly disruptive surges in energetic particle populations in the magnetosphere and rapidly-varying ionospheric- magnetospheric currents that can either completely paralyze or adversely affect the functioning of modern satellites and the large power distribution grids on the ground. The prediction of geomagnetic storms and substorms forms an important basic component of the Space Weather Program. Substorms are the fundamental element in understanding the nature of geomagnetic activity.

7.2. Substorm Phases

An isolated substorm has three phases, namely, growth, expansion, and recovery phase. The magnetosphere attains a kind of ground state (i.e., quiet period) after a prolonged period of northward interplanetary magnetic field (IMF) in the solar wind. The growth phase is identified with the start of southward turning of IMF. During the growth phase, the polar cap size increases as the polar electrojets intensify in the ionosphere. In the magnetosphere, the cross-section of the magnetotail increases, near-earth plasma sheet starts thinning and the dipolar magnetic field is stretched into a tail-like field. At substorm expansion phase, in the midnight sector, there is a sudden brightening of the discrete auroral arcs along with their rapid poleward advancement (see Figure 33). In the near-earth magnetosphere the stretched tail-like configuration relaxes abruptly to a dipolar-like field geometry in association with thickening of the plasma sheet and earthward injection of energetic particles leading to the ring current formation. The cross-tail current is suddenly interrupted and diverted to the polar ionosphere along magnetic field lines. The diverted current flows into the ionosphere on the morning side of the tail, then flows across the auroral ionosphere as the intensified westward electrojet and closes back into the magnetosphere by flowing upward along the field lines on the dusk side of the tail. This pattern of diverted current flow is known as the substorm current wedge (McPherron et al., 1973; Baumjohann, 1986). The recovery phase begins when the poleward expansion of the auroral bulge halts and the auroras start receding equatorward (Akasofu et al., 1966) as shown in Figure 33. The plasma sheet suddenly thickens with fast field-aligned plasma flows in the plasma sheet boundary layers, the B_z component of the magnetic field increases and the strength of high-latitude currents and auroral luminosity decreases. The important events occuring during the three phases of the substorms are summarized in Figure 34.

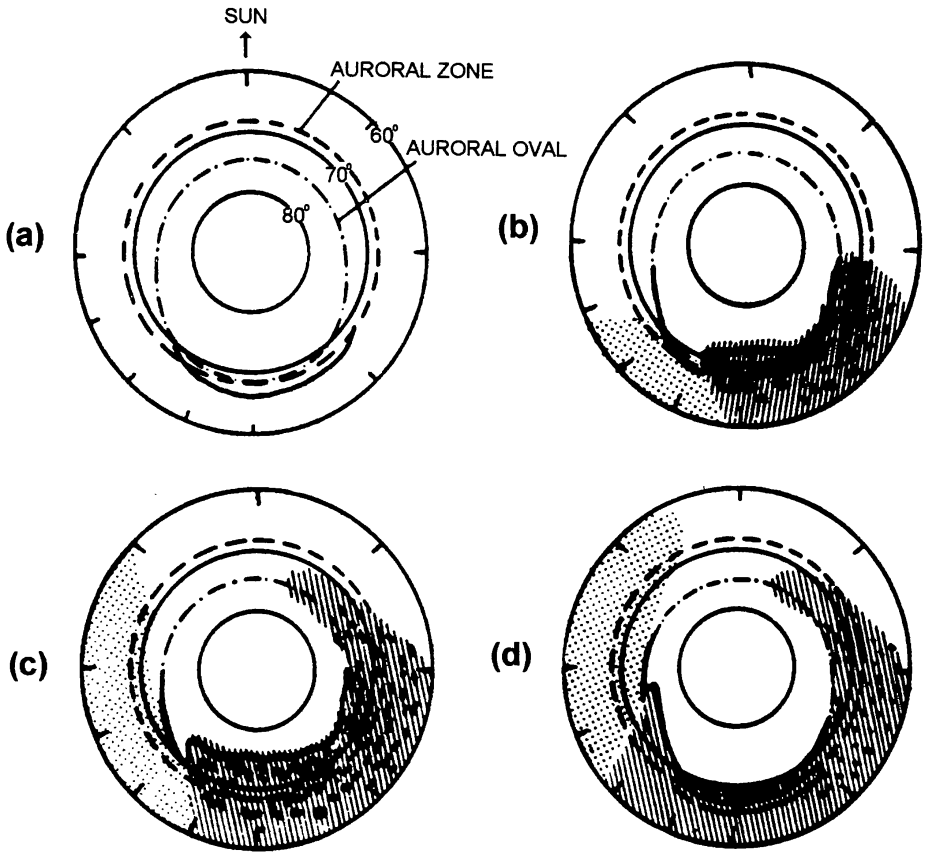

Figure 33. Schematic diagram to show the development of both the auroral and polar magnetic substorms from, (a) a quiet situation, (b) an early epoch of the expansive phase, (c) the maximum epoch of the substorm, to (d) an early epoch of the recovery phase. The region where a negative magnetic bay is observed is indicated by the line shade, and the region of a positive bay by the dotted shade (after *Akasofu et al.* 1966).

7.3. Reconnection Model of the Substorm

A magnetosphseric substorm represents a repeatable sequence of energy loading and subsequent dissipation events on a global scale (Baker et al., 1996; 1998, 1999). Studies based on linear prediction filtering technique indicate that the typical time scales for the driven and loading-unloading processes are about 20 minutes and 1 hour respectively. Several models have been proposed for the substorm phenomena based on the nature of solar wind energy input and that of the stored energy in the magnetosphere (Kan et al., 1991). In fact, the *current disruption model* treats the substorm as a process *directly driven* by the solar wind (Akasofu, 1972). According to this model, the solar wind energy input (equivalent to the power of SM dynamo) directly controls the response of the magnetosphere such as the magnetospheric energy dissipation rate. Here, we shall emphasize the reconnection model of the substorm, also known as the *near-earth neutral line*

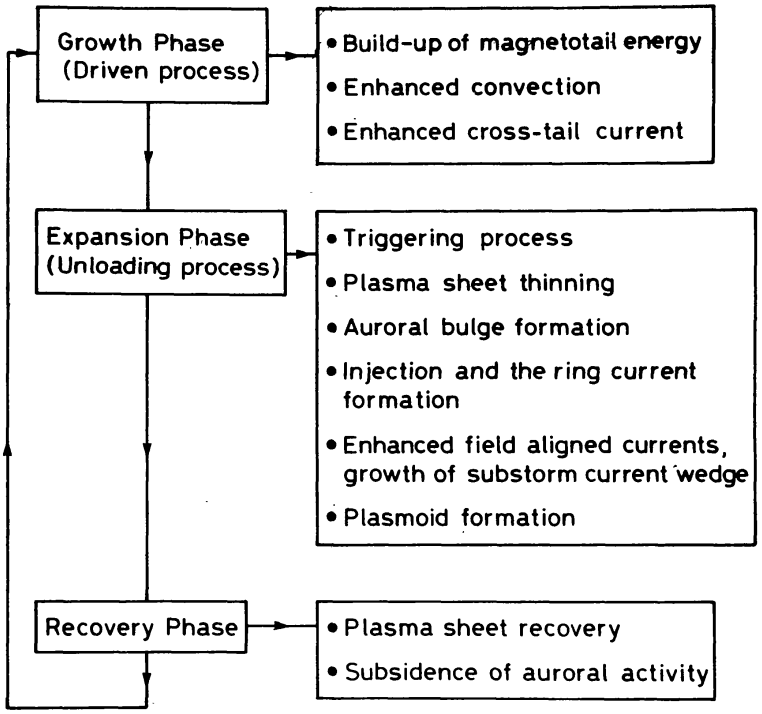

Figure 34. Block diagram showing important events taking place during various phases of a magnetospheric substorm (taken from *Lakhina*, 1993a).

(NENL) model, which is considered to be the most successful model as most of the substorm features can be fitted nicely in its framework.

The *reconnection model* (or NENL model) (Hones, 1977, 1979), treats the substorm phenomenon as a *loading-unloading process.* It describes the growth phase as due to enhanced dayside magnetic reconnection which leads to a larger tail size and thinning of the plasma sheet. The magnetic energy stored in the magnetotail is released explosively through a magnetic reconnection process in the vicinity of a newly formed neutral line in the near-earth tail region (at about 10 - 20 R_E down-stream). The neutral line formation leads to the disruption (actual mechanism is some what uncertain) of the cross-tail current in the vicinity of the neutral line, and to the severence of the plasmasheet to produce a plasmoid. The scenario of events for the near-earth neutral line model is shown in Figure 35. This picture of the substorm can explain many features connected with substorm activity.

The near-earth neutral line (NENL) model faced a major controversy as subsequent observations failed to locate the neutral line near 20 R_E despite the rather overwhelming evidence of substorms typically being initiated there (Lui, 1991).

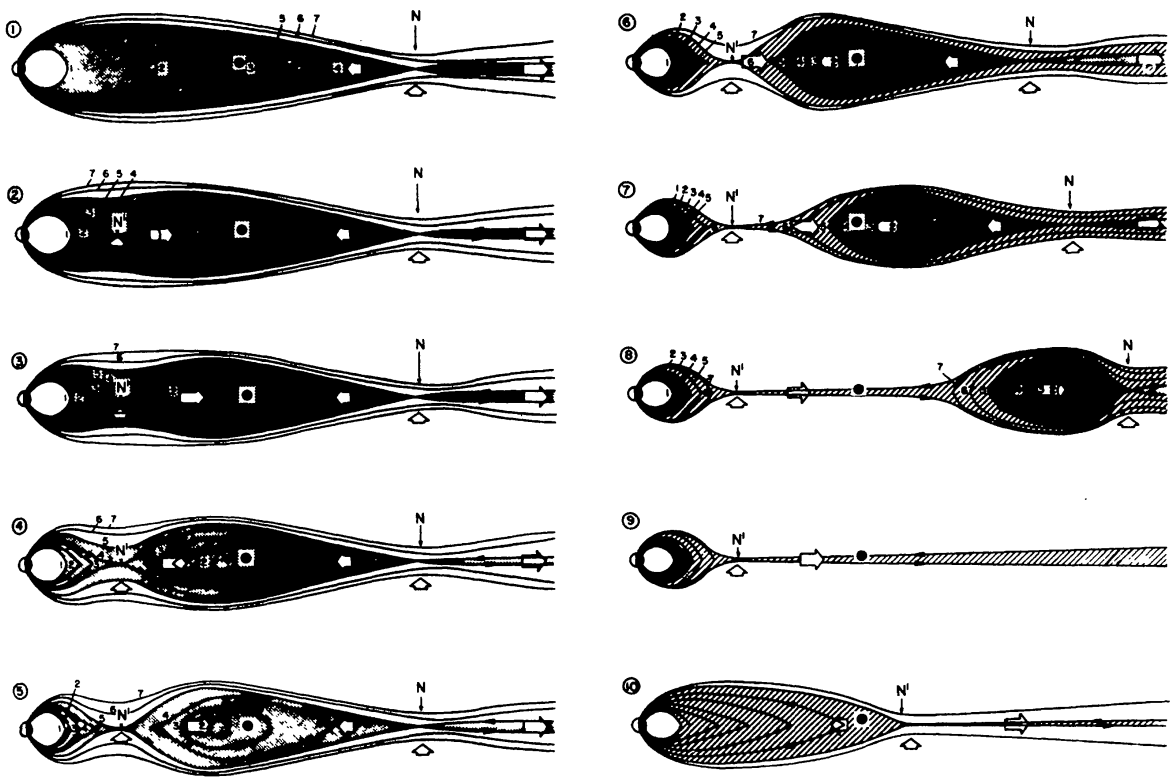

Figure 35. Schematic representation of changes of the magnetotail plasma sheet that are thought to occur during substorms. These are cuts along the midnight meridian plane of the tail. Earth is at left and a dot near the center of each picture represents a satellite at X = - 35 R_E. Black lines are magnetic field lines and white arrows indicate plasma flow. A distant neutral line, N, is shown at X = -60 R_E and is thought to be a quasi-permanent feature of the magnetotail though its distance is not really known and is probably quite variable. The fine hatching indicates the plasma sheet, which contains closed field lines 1, 2, 3, 4 and is bounded by the "last closed field line", 5. Field lines 6 and 7 are in the lobe, outside the plasma sheet (taken from *Hones*, 1977).

However, the latest results from the Geotail mission (Nagai et al., 1998), shown in Figure 36, have provided a strong support to the NENL or reconnection model. The figure clearly shows that fast flows are consistent with magnetic reconnection in the region around $X = -25R_E$, and the global flow pattern is consistent with the NENL model, i.e, plasmoid formation following midtail reconnection (Baker et al., 1996).

How is the near-earth neutral line formed? This is a crucial point concerning the reconnection model. It has been suggested that the substorms neutral line may be formed due to the tearing mode, especially the ion tearing mode instability in the plasmasheet (Coppi et al., 1966; Schindler, 1974, Galeev and Zelenyi, 1976; Lakhina and Schindler 1988, Lakhina, 1992a). However, the tearing mode

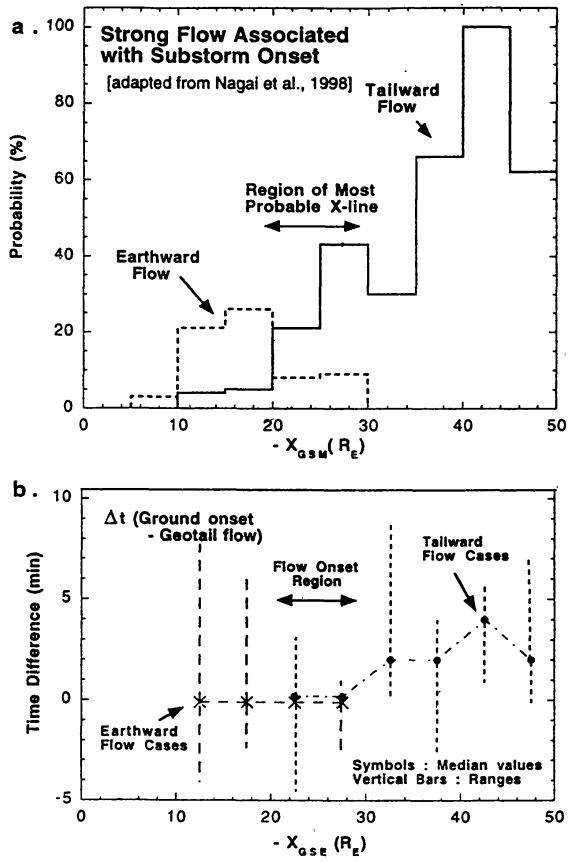

Figure 36. (a) The probability of detecting strong plasma flow ($V > 300$ km s^{-1}) in association with substorm expansion phase onsets. Earthward flow (dashed lines) and tailward flow (solid lines) histograms are shown as a function of X_{GSM} (here X_{GSM} is the x axis in the geocentric solar magnetospheric (GSM) coordinate system)in the tail. The region of most probable neutral line detection is X_{GSM} = -25 R_E . (b) The median (and ranges) of Δt, the time differences between ground substorm onsets and Geotail flow bursts. The prevalence of zero or negative Δt for $-20 \geq X_{GSM} \geq -30 R_E$ suggests that flows originate in that region of the tail (taken from *Nagai et al.*, 1998).

instability tends to get stabilized by the adiabatic electrons in the presence of a normal component, B_n, of the magnetic field (Lembege and Pellat, 1982). Recently it has been suggested that the forced thin current sheet formed during growth phase of the substorm (Fairfield,1984, Mitchell *et al.*, 1990) might become unstable against the ion tearing mode (Burkhart et al., 1992, Burkhart et al., 1993, Lakhina, 1993b) and thus may lead to the substorm onset. The process of driven magnetic reconnection induced by perturbations at the magnetopause boundary has been suggested as another possible mechanism to trigger substorm onset(McPherron et al., 1986; Horton and Tajima, 1988; Lakhina, 1992b, 1994).

Büchner and Zelenyi (1987) proposed that chaotic electron motion might act similar to pitch angle scattering in destabilizing the collisionless tearing mode (Coroniti, 1980) in the magnetotail leading to substorm onset. They showed that

the tearing mode can be unstable when $\kappa_e \simeq 1$, where $\kappa_e = (R_c/\rho_n)$, with R_c as the maximum radius of curvature, and ρ_n as the Larmor radius for electrons. It is interesting to point out that κ_e can decrease from $\kappa_e \gg 1$ to $\kappa_e \simeq 1$ as the magnetotail becomes thinner, and thus it can possibly provide a transition from stability to instability. However, Lui et al.(1992) have found $\kappa_e \simeq 4$ - 10 just prior to the current disruption in the tail, and concluded that their data do not support the substorm onset condition $\kappa_e \simeq 1$. Two-dimensional particle simulations indicate that for $\kappa_e \ll 1$, ion tearing mode is stabilized when $\lambda > \rho_n$ (λ being the wavelength of the tearing mode), a condition which is generally satisfied (Pritchett, 1994). Several effects have been found which can potentially increase the tearing growth rates, for example the development of pressure anisotropy(Chen and Palmadesso, 1984), the presence of shear flow in the plasma sheet boundary layer(Lakhina and Schindler, 1983, 1988), coalescense of magnetic islands(Richard et al., 1989), and the external driving (Horton and Tajima, 1988; Lakhina, 1992b). Some aspects of nonlinear particle dynamics in the magnetotail, e.g., concept of differential memory (Chen and Palmadesso, 1986, 1987) and phase space resonance effect (Burkhart and Chen, 1991, Chen, 1992) have been suggested for the enhancement of the growth rate of the tearing modes. However, destabilization of the tearing mode in the magnetotail is a very controversial topic, and the reader can refer to Pellat et al. (1991) and Kuznetsova and Zelenyi (1991)for more details.

8. Conclusion

Magnetic reconnection has been invoked to explain a multitude of phenomena, observed in space, astrophysical, and laboratory plasmas, which require release of magnetic energy in an explosive manner. Magnetic reconnection appears to be the most likely mechanism by which solar magnetic fields power the solar atmosphere. This is also the likely process by which solar wind flow couples to planetary and cometary magnetospheres leading to the transfer of mass, momentum and energy between the solar wind and the magnetospheres/ionospheres. The International Solar-Terrestrial Physics (ISTP) program which aims to study the Sun-Earth connection has the study of the magnetic reconnection process as one of its key components. Whereas a significant progress has been made in developing theories and simulation codes in 2 dimensions, the studies on 3 D magnetic reconnection are rather few and far between. There is an urgent need to develop sophisticated 3D simulation codes capable of handling large magnetic Reynolds numbers and complicated magnetic configurations. In the new millennium, one would expect to see more exotic applications of magnetic reconnection to pulsars, stellar accretion disks, active galactic nuclei, and gamma ray bursts.

References

Akasofu, S.I., Meng, C.I. and Kimball, D.S., 1966, J. Atmos. Terr. Phys., 28, 505.

Akasofu, S.I., 1972, in Solar Terrestrial Physics, edited by E.R. Dryer, D. Reidel, Norwood, Mass, Part III, p.131.

Antiochos, S. K., and C. R. DeVore, 1999, in Sun-Earth Plasma Connection, Geophysical Monogram 109, eds. J. L. Burch, R. L. Carovillano and S. K. Antiochos, American Geophysical Union, Washington D.C., p. 113.

Axford, W. I., in Magnetic Reconection in Space and Laboratory Plasmas, edited by E. W. Hones, Jr., AGU, Washington, DC, 1984, p. 1.

Baker, D. N., T. I. Pulkkinen, V. Angelopoulos, W. Baumjohann, and R. L. McPherron, 1996, J. Geophys. Res., 101, 12975.

Büchner, and A. J. Klimas, 1998, in Substorms-4, edited by S. Kokubun, and Y. Kamide, Terra Scientific, Tokyo, p. 231.

Büchner, and A. J. Klimas, 1999, J. Geophys. Res., 104, 14601.

Baumjohann, W., 1986, J. Geomagn. Geoelectr., 38, 633.

Biernat, H. K., M. F. Heyn, R. P. Rijnbeck, V. S. Semenov, and C. J. Farrugia, 1990, Ann. Geophys., 8, 69.

Birn, J. and E. W. Hones, Jr., 1981, J. Geophys. Res., 86, 6802.

Birn, J. and M. Hesse, 1991, J. Geophys. Res., 96, 1611.

Büchner, J., and L. M. Zelenyi, 1987, J. Geophys. Res., 92, 13456.

Burkepile, J. T., and O. C. St. Cyr, 1993, A Revised and Expanded Catalogue of Mass Ejections Observed by the Solar Maximum Mission Coronagraph, HAO.

Burkhart, G. R., and Chen, J., 1991, J. Geophys. Res., 96, 14,033.

Burkhart, G. R., J. F. Drake, P. B. Dusenbery, and T. W. Speiser, 1992, J. Geophys. Res., 97, 13799.

Burkhart, G. R., Dusenbery, P. B., Speiser, T. W. and Lopez, R. E., 1993, J. Geophys. Res., 98, 21373.

Carmichael, H., 1964, in AAS-NASA Symposium on Physics of Solar Flares, ed. W. N. Hess (NASA-SP 50), Washington D.C., p. 451.

Chen, X. L. and P. J. Morrison, 1990, Phys. Fluids, B2, 495.

Chen, J., and P. Palmadesso, 1984, Phys. Fluids, 27, 1198.

Chen, J. and Palmadesso, P.J., 1986 , J. Geophys. Res., 91, 1499. (correction, 1986, J. Geophys. Res., 91, 9025).

Chen, J., and Palmadesso, P.J., 1987 in Magnetotail Physics, edited by A.T.Y. Liu, The John Hopkins University Press, Baltimore, Md., , p 321.

Chen, J., 1992, J. Geophys. Res., 97, 15,011.

Coppi, B., G. Laval, and R. Pellat, 1966, Phys. Rev. Lett, 16, 1207.

Coroniti, F. V., 1980, J. Geophys. Res., 85, 6719.

Cowley, S. W. H., 1985, in Solar System Magnetic Fields, edited by E. R. Priest, D. Reidel Publishing Company, Dordrecht, Holland, p. 121.

Craig, I. J. D., 1981, in Solar Flare Magnetohydrodynamics, ed. E. R. Priest, Gordon and Breach, London, P. 277.

Dungey, J. W., 1961, Phys. Rev. Lett., 6, 47.

Dungey, J. W., 1978, J. Atmos. Terr. Phys., 40, 231.

Fairfield, D. H., 1984, in Magnetic Reconnection in Space and Laboratory Plasmas, edited by E.W. Hones, Jr., Geophys. Monogr., vol. 30, AGU, Washington, D. C., p. 168.

Forbes, T. G., and R. R. Priest, 1987, Revs. Geophys. , 25, 1583.

Forbes, T. G., and R. R. Priest, 1984, Solar Phys., 94, 315.

Furth, H.P., J. Killeen and R.M. Rosenbenth, 1963, Phys. Fluids, 6, 459.

Galeev, A. A., and Zelenyi, L.M., 1976, Sov. Phys. JETP, Engl. Transl., 43, 1113.

Galeev, A.A., 1984, in Handbook of Plasma Physics, Vol. 2, edited by M.N. Rosenbluth and R.Z. Sagaeev, North Holland, Amsterdam, p 305.

Giovanelli, R. G., 1947, Mon. Notice Roy. Astron. Soc., 107, 338.

Gonzalez, W. D., Joselyn, J. A., Kamide, Y., Kroehl, H. W., Rostoker, G., Tsurutani, B. T., and Vasyliunas, V. M., 1994, J. Geophys. Res., 99, 5771.

Gratton, F. T., M. F. Heyn, H. K. Biernat, R. P. Rijnbeek, And G. Gnavi, 1988, J. Geophys. Res., 93, 7318.

Greene, J. M., 1988, J. Geophys. Res., 93, 8583.

Hameiri, E., 1979, *J. Plasma Phys.*, 22, 245.

Hautz, R. and M. Scholer, 1987, Geophys. Res. Lett., 14, 967.

Hesse, M., and K. Schindler, 1988, J. Geophys. Res., 93, 5559.

Heyvaert, J. E. R. Priest, and D. M. Rust, 1977, Astrophys. J., 216, 123.

Hirayama, T., 1974, Solar Phys., 34, 323.

Hones, E.W., Jr., 1977, comments on, " On hot tenuous plasmafireballs and boundary layers in the earth's magnetotail", by L. A. Frank, L. L. Ackerson and R. P. Lepping, J. geophys. Res., 82, 5633.

Hones, E.W., Jr., 1979, Space Sci. Revs., 23, 393 - 410.

Horton, W. and T. Tajima, 1988, Geophys. Res. Lett., 17, 2741.

Howard, R., and Svestka, Z., 1977, Solar Phys., 54, 65.

Hudson, H. S., 1994, in Proc. Kofu Meeting, eds. S. Enome and T. Hirayama, Nobeyama Radio Observatory, p. 1.

Kamide, Y. and Kroehl, H. W., 1994, Geophys. Res. Lett., 21, 389.

Kan, J. R., Potembra, T. A., Kokubun S. and Iijima, T., 1991, Magnetospheric Substorms, Geophysical Monograph, 64, American Geophysical Union, Washington, D. C.

Kasugi, T., K. Makishima, T. Murakami, T. Sakao, t. Dotani, M. Inda, K. Kai, S. Masuda, H. Nakajima, Y. Ogawara, M. Sawa, And K. Shibasaki, 1991, Solar Phys., 136, 17.

Kopp, R. A. and Pneuman, G. W., 1976, Solar Phys., 50, 85.

Kundu, M. R., 1985, in Unstable Current Systems and Plasma Instabilities in Astorphysics, eds., M. R. Kundu and G. D. Holman, IAU Symposium No. 107, D. Reidel, Dordrecht, Holland, p.185.

Kuznetsova, M. M. and Zelenyi, L.M., 1991, Geophys. Res. Lett., 18, 1825.

Lakhina, G. S., and K. Schindler, 1983, Astrophys. Space Sci., 89, 293.

Lakhina, G. S. and K. Schindler, 1988, J. Geophys. Res., 93, 8591.

Lakhina, G. S., 1992a, in Memoirs of Geophysical Society of India, No.24, Bangalore, India, p. 307.

Lakhina, G. S., 1992b, J. Geophys. Res., 97, 2961.

Lakhina, G. S., 1993a, J. Geophys. Res., 98, 17409.

Lakhina, G. S., 1993b, Bull. Astr. Soc. India, 21, 537.

Lakhina, G. S., 1994, Surveys Geophys., 15, 703.

Lakhina, G. S., and B. T. Tsurutani, 1998a, Phys. News, 29, 5.

Lakhina, G. S., and B. T. Tsurutani, 1998b, Physica Scripta, T74, 67.

Lee, L. C., and Z. F. Fu, 1985, Geophys. Res. Lett., 12, 105.

Lee, L. C., and Z. F. Fu, 1986, J. Geophys. Res., 91, 6807.

Lee, L. C., Z. W. Ma, Z. F. Fu, and A. Otto, 1993, J. Geophys. Res., 98, 3943.

Lembege, B., and R. Pellat, 1982, Phys. Fluids, 25 , 1995.

Liu, Z. X., and Y. D. Hu, 1988, Geophys. Res. Lett., 15, 752.

Lui, A. T. Y., Lopez, R.E., Anderson, B.J., Takahashi, K., Zanetti, L.J., McEntire, R.W., Potemra, T.A., Klumpar, D.M., Greene, E.M. and Strangeway, R., 1992, J. Geophys. Res., 97, 1461.

Lui, A. T. Y., 1991, J. Geophy. Res., 96, 1849.

Ma, Z. W., A. Otto, and L. C. Lee, 1994, J. Geophys. Res., 99, 6125.

Masuda, S., T. Kosugi, H. Hara, T. Sakao, K. Shibata, and S. Tsuneta, 1995, Publ. Astron. Soc. Japan, 47, 677.

McPherron, R.L., Russell, C.T. and Aubry, M.D., 1973, J. Geophys. Res., 78, 3131.

McPherron, R. L., Terasawa, T. and Nishida, A., 1986, J. Geomagn. Geoelectr., 38, 1098.

Mitchell, D. G., Williams, D. J., Huang, C. Y., Frank, L. A., and Russell, C. T., 1990, Geophys. Res. Lett., 17, 583.

Nagai, T., M. Fujimoto, Y. Sato, S. Machida, T. Terasawa, R. Nakamura, T. Yamamoto, T. Mukai, A. Nishida, and S. Kokubun, 1998, J. Geophys. Res., 103, 4419.

Nishida, A., 1989, Geophys. Res. Lett., 16, 227.

Ogawara, Y., T. Takano, T. Kato, T. Kasugi, S. Tsuneta, T. Watanabe, I. Kondo, Y. Uchida, 1991, Solar Phys., 136, 1.

Ogino, T., R. J. Walker, and M. Ashour-Abdalla, 1990, in Physics of Magnetic Flux Ropes, Geophys. Monograph 58, edited by C. T. Russell, E. R. Priest and L. C. Lee, AGU, Washington D.C., p.669.

Ohyama. M. and K. Shibata, 1997, Publ. Astron. Soc. Japan, 49, 249.

Otto, A., 1991, Geophys. Astrophys. Fluid Dyn, 62, 69.

Parker, E. N., 1957, J. Geophys. Res., 62, 509.

Parker, E. N., 1988, Astrophys. J., 330, 474.

Pellat, R., Coroniti, F.V. and Pritchett, P.L., 1991, Geophys. Res. Lett., 18, 143.

Petschek, H. E., 1964, in NASA Special Publ., NASA - SP - 50, p. 425.

Pneuman, G. W., 1980, in *Solar and Interplanetary Dynamics*, eds., M. Dryer and E. Tandberg- Hanssen, IAU Symposium No.91, D. Reidel, Dordrecht, Holland, p.317.

Priest, E. R., 1981, ed. Solar Flare Magnetohydrodynamics, Vol.1, Gordon and Breach Science Publishers, New York.

Priest, E. R., and T. G. Forbes, 1986, J. Geophys. Res., 91, 5579.

Pritchett, P. L., 1994, J. Geophys. Res., 99, 5935.

Richard, R. L.,R. J. Walker, R. D. Sydora, and M. Ashour-Abdalla, 1989, J. Geophys. Res., 93, 2471.

Russell, C. T. and R. C. Elphic, 1978, Space Sci. Rev., 22, 681.

Schindler, K., 1974, J. Geophys. Res., 79, 2803.

Schindler, K., 1984, in Magnetic Reconection in Space and Laboratory Plasmas, edited by E. W. Hones, Jr., AGU, Washington, DC, p. 9.

Schindler, K., M. Hesse, and J. Birn, 1988, J. Geophys. Res., 93, 5547.

Shay,M. A., J. F. Drake, B. N. Rogers, and R. E. Denton, 1999, Geophys. Res. Lett., 26, 2163.

Shibata, K., S. Masuda, M. Shimojo, et al., 1995, Astrophys. J., 451, L83.

Shibata, K., 1996, Adv. Space Res., 17, no. 4/5, 9.

Sonnerup, B. U. Ö, 1970, J. Plasma Phys., 4, 161.

Sonnerup, B. U. Ö and E. R. Priest, *J. Plasma Phys.*, 1975, 14, 283.

Sonnerup, B. U. Ö, J. Ip, and T. D. Phan, 1990, in Physics of Magnetic Flux Ropes, edited by C. T. Russell, E. R. Priest, and L. C. Lee, Geophys. Monogr. 58, AGU, Washington, DC, p. 63.

Speiser, T. W., 1965, J. Geophys. Res., 70, 4219.

Sturrock, P. A., 1973, in High Energy Phenomena on the Sun, Eds. R. Ramaty and R. G. Stone, p. 3.

Sturrock, P. A., 1974, in Flare related Magnetic Field Dynamics, (eds.)Y. Nakagawa and D M. Rust, N. C. A. R., Boulder, Colorado.

Sturrock, P. A., T. E. Holzer, D. M. Mihalas, and R. K. Ulrich, 1986, eds, Physics of the Sun, Volume II: The Solar Atmosphere, D. Reidel Publishing Company, Dordrecht,

Svestka, Z., B. V. Jackson, M. E. Machado, Editors, 1992, Eruptive Solar Flares, Springer-Verlag, Berlin, Heidelberg.

Sweet, P. A., 1958, in Electromagnetic Phenomena in Cosmical Physics, edited by B. Lehnert, Cambridge University Press, New York, p. 123.

Tajima, T., Brunel, F., Sakai, J.-I., Vlahos, L. and Kundu, M. R., 1985, in Unstable Current Systems and Plasma Instabilities in Astorphysics, eds., M. R. Kundu and G. D. Holman, IAU Symposium No. 107, D. Reidel, Dordrecht, Holland, p.197.

Tsuneta, S., T. Takahashi, L. W. Acton,M. E. Bruner, K. L. Harvey, and Y. Ogawara, 1992, Publ. Astron. Soc. Japan., 44, L211.

Tsuneta, S., 1996, Astrophys. J., 456, 840.

Uberoi, C., L. J. Lanzerotti, and A. Wolfe, 1996, J. Geophys. Res., 101, 24979.

Vasyliunas, V. M., 1975, Rev. Geophys., 13, 303.

White, R. B., 1983, in Handbook of Plasma Physics, vol. 1, edited by M. N. Rosenbluth and R. Z. Sagdeev, North-Holland, Amsterdam, P.611.

Yan, M., L. C. Lee, and E. R. Priest, *J. Geophys. Res.*, 1992, 97, 8277.

Yeh, T., and W. I. Axford, 1970, J. Plasma Phys., 4 , 207.

Yokoyama, T. and K. Shibata, 1995, Nature, 375, 42.

Yokoyama, T. and K. Shibata, 1996, Publ. Astron. Soc. Japan, 48, 353.

Zelenyi, L. M., and M. M. Kuznetsova, 1984, Sov. J. Plasma Phys., 10, 190.

Zwingmann, W., J. Wallace, K. Schindler, and J. Birn, 1990, J. Geophys. Res., 95, 20877.